JCI The Journal of Clinical Investigation

Long noncoding RNA HITT coordinates with RGS2 to inhibit PD-L1 translation in T cell immunity

Qingyu Lin, … , Hao Liu, Ying Hu

J Clin Invest. 2023. https://doi.org/10.1172/JCI162951.

Research In-Press Preview Immunology Oncology

Graphical abstract

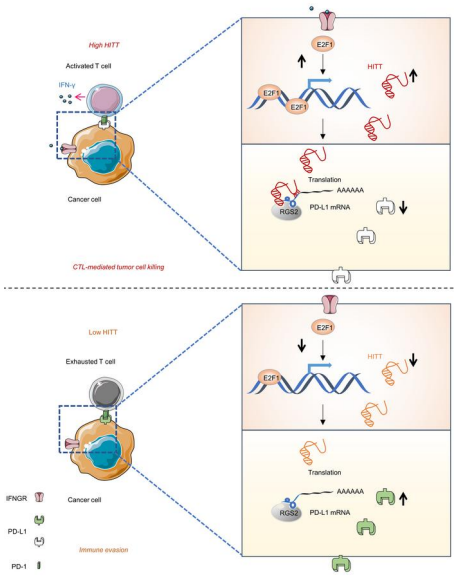

Find the latest version:

https://jci.me/162951/pdf

Long noncoding RNA HITT coordinates with RGS2 to inhibit PD-L1 translation in T cell immunity

Qingyu Lin[1*], Tong Liu[2*], Xingwen Wang[1], Guixue Hou[3], Zhiyuan Xiang[1], Wenxin Zhang[1], Shanliang Zheng[1], Dong Zhao[1], Qibin Leng[4], Xiaoshi Zhang[5], Minqiao Lu[1], Tianqi Guan[1], Hao Liu[1], Ying Hu [1*]

1 School of Life Science and Technology, Harbin Institute of Technology, Harbin, Heilongjiang Province, China, 150001

2 Department of Breast Surgery, Harbin Medical University Cancer Hospital, Harbin, China; Heilongjiang Academy of Medical Sciences, Harbin, China.

3 BGI-SHENZHEN, Shenzhen, 518083, China.

4 Affiliated Cancer Hospital and Institute of Guangzhou Medical University, State Key Laboratory of Respiratory Disease, 78 Heng Zhi Gang Road, Guangzhou 510095, China.

5 Department of Clinical Laboratory, Qilu Hospital of Shandong University, Jinan, Shandong, China 250012

Conflict of interest: The authors have declared that no conflict of interest exists.

* These authors contribute equally to the work.

Address correspondence to: School of Life Science and Technology, Harbin Institute of Technology, 150001 Harbin, Heilongjiang Province, China. Tel: 0086-86403826. Email: huying@hit.edu.cn.

Abstract

Programmed death ligand 1 (PD-L1) is an immune checkpoint protein frequently expressed in human cancers, which contributes to immune evasion through its binding to PD-1 on activated T cells. Unveiling the mechanisms underlying PD-L1 expression is essential for understanding the impacts of immunosuppressive microenvironment, and also crucial for the purpose of re-boosting anti-tumour immunity. However, how PD-L1 is regulated, particularly at translational levels, remains largely unknown. Here, we discovered that a lncRNA, HIF-1α inhibitor at translation level (HITT), was transactivated by E2F1 under interferon-γ stimulation. It bound and co-ordinated with Regulator of G Protein Signalling 2 (RGS2) in binding to the 5'-untranslated region (UTR) of *PD-L1*, resulting in reduced PD-L1 translation. HITT expression enhanced T cell-mediated cytotoxicity both

in vitro and in vivo in a PD-L1 dependent manner. The clinical correlation between HITT/PD-L1, RGS2/PD-L1 expression was also detected in breast cancer tissues. Together, these findings demonstrate the role of HITT in antitumour T cell immunity, highlighting activation of HITT as a potential therapeutic strategy to enhance cancer immunotherapy.

Introduction

Immune escape is a hallmark of cancer evolution, involving a complex interplay between tumour cells and the host immune microenvironment, and is a central modifier of clinical outcomes(1). Cancer cells gain this fundamental trait by exploiting a plethora of immunosuppressive pathways, such as the induction of immune checkpoints, as exemplified by programmed cell death ligand 1 (PD-L1)(2). PD-L1 binds with programmed cell death-1 (PD-1), a key immune checkpoint protein expressed on the surface of activated T cells, leading to suppressed cytotoxic T cell activity(3). Unsurprisingly, immunotherapies that aim to achieve immune checkpoint blockade by targeting the PD-1/PD-L1 interaction have yielded striking clinical benefits in advanced malignancies(4, 5). Nevertheless, only a small fraction (20–40%) of patients benefit from PD-1/PD-L1 blockade therapies(6). Compared with others, PD-L1 expression is considered as a relative reliable predictor of response to treatment(7), despite with exceptions(8). Thus, it is essential that we understand how PD-L1 is regulated, because it may lead to not only response predictors of PD-1/PD-L1 blockade, but also alternative strategies to target the PD-1/PD-L1 pathway. Recently, mounting evidence has suggested that PD-L1 expression is regulated at multiple levels; however, how translational processes influence PD-L1 protein output remains poorly understood(4).

Regulator of G Protein Signalling 2 (RGS2) belongs to a family of proteins that participate in the G protein cycle(9). Like its family members, RGS2's function is the inactivation of G protein signalling by serving as a GTPase activating protein(9, 10). This activity requires a canonical RGS domain that is shared by all family members(9, 10). In line with its role in inhibiting G protein signalling, RGS2 knockout mice studies have revealed that it is essential in the cardiovascular and central nervous systems(11, 12). However, G protein signalling cannot explain all of the physiological functions of

RGS2, leading to extensive effort to elucidate the molecular mechanisms of noncanonical RGS2 functions. As such, an increasing number of protein-binding partners, in addition to G protein, have been discovered(13). These additional functions, which include angiogenesis, migration, and chronic inflammation, have led to the discovery of RGS2's role in cancer pathology(14, 15). Although the underlying mechanisms and pathological significance remain largely unexplored, a novel function of RGS2 in regulating mRNA translation has also been reported(16). Moreover, RGS2 has been shown to be induced in activated T cells, and have a bronchoprotective role in a murine model of lipopolysaccharide (LPS)-induced airway inflammation(17, 18). However, how RGS2 regulates T cell immunity and whether it has a role in the context of cancer immunity are not yet understood.

Long noncoding RNAs (lncRNAs) are a class of RNA arbitrarily defined as RNA molecules longer than 200 nucleotides with limited protein-coding potential(19). In-depth studies suggest that lncRNAs exert their biological activities by forming complexes with mRNA, DNA, or proteins(20). A growing body of work shows that lncRNAs are key regulators in diverse physiological and pathological contexts, including cancer(21). However, although much has been learned about the multiple functions of lncRNAs in cancer cell proliferation, apoptosis, invasion, and migration, little is known about their potential to regulate immune evasion(21).

Previous work by our group identified a lncRNA named HIF-1α inhibitor at translation level (HITT), also known as linc00637 or PPP1R13B divergent transcript (PPP1R13B-DT)(22). By analysing The Cancer Genome Atlas (TCGA) database and in-house samples, HITT was found to be downregulated in multiple types of cancer and decreased HITT expression is associated with advanced stages of colon, bladder, breast, and liver cancers. Mechanistically, HITT elicits remarkable antitumour effects by modulating cells' responses to hypoxia and DNA damage through inhibiting HIF-1α synthesis and ATM activity, respectively(22, 23). It is also worth noting that, in addition to hypoxia and DNA damage, cancer cells are inevitably insulted under inflammatory microenvironment conditions. Pro-inflammatory cytokines, like interferon-γ (IFN-γ), tumour necrosis factor (TNF)-α,

granulocyte–macrophage colony-stimulating factor (GM-CSF), and interleukin (IL)-10 secreted in the inflammatory tumour microenvironment, are regarded to be important triggers of PD-L1 expression(4, 24). This is in line with the well-established connection between inflammation, immune evasion, and carcinogenesis. Thus, it will be of interest whether and how HITT, as a cancer-related stress responder, is involved in regulating T cell immunity in cancer.

Results

HITT promotes T cell immunity

We first compared the anti-cancer effects of HITT in immune-competent BALB/c mice treated with anti-CD8α antibody to block CD8+ T cells cytotoxicity or the IgG control (Figure 1, A-C). As expected, murine mammary carcinoma 4T1 grow more quickly in mice treated with anti-CD8α antibody than in the mice treated with IgG isotype control (Figure 1, A-C). HITT overexpression in 4T1 cells attenuated tumour growth under both conditions (Figure 1, A-C). Whereas it suppressed tumour growth more evidently in the control mice (HITT/vector control: 25-34%) than in anti-CD8α antibody-treated mice (HITT/vector control: 78-80%) (Figure 1, A-C). This is not due to the different HITT fold changes (Figure 1D). In line with above data, 3-(4,5-Dimethylthiazol-2-yl)-2,5-diphenyltetrazolium bromide (MTT) and 5-bromo-2'-deoxyuridine) (BrdU) incorporation assays reveled no obvious intrinsic impacts of HITT on the cell viability and proliferation in 4T1 cells (Supplemental Figure 1, A and B). Inspired by this observation, the effects of HITT expression by cancer cells on T cell activity were further explored. MDA-231 (breast cancer) and HeLa (cervical cancer) cells stably expressing HITT and vector controls were successfully established and validated by quantitative (q)RT-PCR (Supplemental Figure 1C). $CD8^+$ T cells were isolated from human blood and activated as described previously(25), and then co-cultured with the established cancer cell lines (Figure 1E). HITT overexpression by cancer cells elevated CTL activity, as indicated by

increased secretion of IL-2 and IFN-γ in the culture medium (Figure 1F). In agreement, HITT-overexpressing cells also exhibited increased vulnerability to CTL attack (Figure 1G). CRISPR/Cas-mediated-HITT knockout (KO) produced opposing results regarding both IL-2 and IFN-γ secretion and T cell-mediated cancer-killing effects (Figure 1 H, I, and Supplemental Figure 1D). Thus, HITT expression by cancer cells plays an important role in promoting T cell immunity.

HITT inhibits PD-L1 expression

To understand how HITT attenuates T cell immunity, we compared mass-spectrum data in the control and HITT KD HeLa cells. Unsupervised hierarchical-clustering analyses show that the HITT KO samples were clustered separately with the controls (Supplemental Figure 1E). A volcano plot demonstrates that 69 proteins were differentially regulated by HITT KO using a threshold of *P* value ≤ 0.05 and fold-change ≥ 1.8, with PD-L1 as one of top hits (Supplemental Figure 1F). As such, the impacts of HITT on PD-L1 expression were explored. Remarkably, PD-L1 was dramatically reduced in HITT-overexpressing human breast cancer cell (MDA-231, MDA-468 and BT549), mouse mammary cancer cell (4T1), cervical cancer cell (HeLa), and colon cancer cell (HT29) (Figure 2A and Supplemental Figure 1G). In contrast, HITT KO or small interfering RNAs (siRNAs)-mediated HITT KD led to increased PD-L1 expression (Figure 2B and Supplemental Figure 1G). Restoration of HITT expression abolished HITT KD-mediated PD-L1 elevation (Supplemental Figure 1H), while the expression of another family member, PD-L2, was unaffected (Figure 2, A and B). PD-L1 localisation was not changed by HITT (Supplemental Figure 1I). Therefore, HITT mainly regulates PD-L1 by repressing its expression, but not by changing its localization.

Intriguingly, HITT expression was increased in a dose- and time-dependent manner in response to IFN-γ exposure in MDA-231 and HeLa cells (Figure 2, C and D). In addition, IFN-γ-induced HITT expression was relatively common, because treatment led to increased HITT expression in all breast cancer cell lines tested regardless of their genetic features (Supplemental Figure 2A and Supplemental Table 1). IFN-γ-induced HITT expression was also observed in lung cancer cells, such

as H23 and H1299 (Supplemental Figure 2A). These data suggest that HITT is a newly identified IFN-γ signal-responsive lncRNA. In addition, we observed that PD-L1 expression was increased by IFN-γ, whereas two independent siRNAs-mediated HITT KD augmented IFN-γ-induced PD-L1 expression (Figure 2E). Therefore, HITT plays important roles in attenuating PD-L1 expression under both basal and IFN-γ-stimulated conditions.

E2F1 transactivates HITT upon IFN-γ stimulation

Given the essential role of HITT in regulating PD-L1 expression, we further explored the underlying mechanisms of IFN-γ-induced HITT expression. HITT promoter luciferase reporter and luciferase-HITT reporter were generated (Supplemental Figure 2B). HITT promoter-driven luciferase activity was elevated in a dose- and time-dependent manner following IFN-γ treatment (Figure 2, F and G), while luciferase-HITT reporter activity was unchanged under the same conditions (Supplemental Figure 2C), suggesting that HITT is activated by IFN-γ at the transcriptional level. In line with these results, actinomycin D (ActD), an mRNA synthesis inhibitor, abolished IFN-γ-induced HITT expression (Supplemental Figure 2D).

We then analysed the UCSC Genome Browser chromatin immunoprecipitation (ChIP) sequencing database (Figure 2H). The most potent transcription factors were Early Growth Response 1 (EGR1), TATA-box binding protein associated factor 1 (TAF1), and E2F Transcription Factor 1 (E2F1) (Figure 2H). IFN-γ treatment barely affected the expression of EGR1 (Supplemental Figure 2E). Despite detecting increased levels of TAF1 in a time-dependent manner after IFN-γ treatment, diminishing its expression by siRNA failed to influence HITT levels (Supplemental Figure 2F). In contrast, E2F1 was remarkably enhanced by IFN-γ in a dose- and time-dependent manner, accompanied by a co-ordinate increase of HITT expression (Figure 2I). Inhibition of E2F1 expression by two independent si-E2F1s completely abolished IFN-γ-induced HITT expression and HITT promoter luciferase activity (Figure 2J).

In addition, ectopic E2F1 expression increased HITT levels and HITT promoter-driven luciferase activity in an E2F1 dose-dependent manner (Supplemental Figure 2G), while KD of endogenous

E2F1 reduced them (Supplemental Figure 2H). Furthermore, the activity of mutant type (MT)1 luciferase reporter, which contains the predicted E2F1-binding sites, was as effective as wild type (WT) reporter in response to E2F1 expression (Figure 2K), whereas MT2 luciferase reporter, without the predicted binding motif, largely lost its response to E2F1. Moreover, binding between E2F1 and the HITT promoter region was verified by a ChIP assay, and binding was increased after IFN-γ treatment (Figure 2L). Taken together, E2F1 is required for transcriptional activation of its target HITT upon IFN-γ stimulation.

HITT and RGS2 co-ordinately inhibit PD-L1 translation

Meanwhile, considering the essential role of PD-L1 in immune evasion, we investigated the mechanisms underlying HITT-inhibited PD-L1 expression. First, we found no obvious change in the expression of *Cd274* mRNA, encoding for PD-L1, after HITT overexpression or KD (Supplemental Figure 3, A and B). Secondly, neither lysosome inhibitor chloroquine nor proteasome inhibitor MG132 influenced HITT-mediated PD-L1 inhibition (Supplemental Figure 3, C and D). Intriguingly, a Click chemistry and L-azidohomoalanine (AHA)-label assay revealed that HITT overexpression inhibited newly synthesised PD-L1 protein (lanes 1 and 2, Figure 3A), while HITT KD promoted it (lanes 1, 3 and 5, Figure 3B), with the newly synthesised HSP90 serving as a negative control (Figure 3, A and B).

It is reasonable to suppose that HITT may fulfil its roles by cooperating with translational regulators. To test this hypothesis, we first utilised the Gene Ontology (GO) database to search translational regulators in the genome. In total, 78 proteins were identified to be negatively involved in protein translation. Among them, we identified 15 proteins that have been reported to be directly or indirectly related to T cell immunity via a literature search (Supplemental Table 2). We then used RNA interference techniques to specifically inhibit the expression of those individual genes (Supplemental Figure 4A). The KD efficiency was verified in each case by qRT-PCR. WB assay revealed an obvious increase of PD-L1 protein expression in the (RGS2) KD cells, but not others (Figure 3C and Supplemental Figure 4A). Intriguingly, the ability of HITT to regulate PD-L1

expression was largely diminished by RGS2 KD (Figure 3C). RGS2 had little effect on PD-L1 expression on the mouse cell line 4T1, which does not contain HITT, and overexpression of HITT in 4T1 cells restored the effects of RGS2 KD on PD-L1 expression (Supplemental Figure 4B). Furthermore, the Click chemistry and AHA-label assay showed that RGS2 KD increased the levels of the newly synthesised PD-L1 protein (lanes 3 and 4, Figure 3A) and also abolished HITT overexpression-inhibited PD-L1 expression (lane 5, Figure 3A). By contrast, RGS2 over-expression repressed the newly synthesized PD-L1 protein (lanes 1 and 2, Figure 3B) and also rescued HITT KD-induced PD-L1 expression (lanes 4 and 6, Figure 3B). Coordinated regulation of PD-L1 translation by RGS2 and HITT was further validated by a chromosome fractionation assay (Figure 3, D and E). Namely, RGS2 and HITT similarly reduced polysome-occupied *Cd274* mRNA and no further reduction was observed with their combination (Figure 3E). These data suggest that HITT and RGS2 co-ordinately regulate PD-L1 translation through the same mechanism.

(1080-1130 nt) HITT is physically associated with F194, Q196, and D197 in the RGS domain of RGS2

Given their coordinated effects on PD-L1 translation, we speculated that HITT may bind with RGS2. Indeed, a UV Cross-Linking and Immunoprecipitation (CLIP) assay (Figure 4A) revealed that HITT and RGS2 physically associate with each other in living cells, and their association was increased after ectopic HITT overexpression (Figure 4B). Consistently, their binding was increased by IFN-γ, while inhibition of IFN-γ-induced HITT expression by si-HITT abolished such an effect (Figure 4C and Supplemental Figure 4C). Direct binding between HITT and RGS2 was also validated by RNA pull-down assay using in vitro-synthesised Biotinylated HITT and purified RGS2 protein, and their binding was suppressed by antisense HITT (Figure 4, D and E).

The key RGS2 binding region in HITT was initially mapped to F3-1 (1030-1247 nt) by in vitro binding assay (Supplemental Figure 5A). After that, this fragment was sequentially truncated to four 100nt fragments with 50nt sequence overlap (F3-1.1~4, Figure 4F). Among those, F3-1.1(1030-1130 nt) and F3-1.2(1080-1180 nt) bound with RGS2 to similar extends, suggesting that their overlapping

region mapped to (1080-1130 nt) contains the key nucleotides in binding RGS2 (Figure 4F). No other HITT F3-1 fragmented mutants (F3-1.3 and F3-1.4) were found to bind with RGS2 (Figure 4F). By mixing truncated RGS2 protein with HITT, we found that C-terminal RGS2 (80-212aa), containing the RGS domain, is necessary for its binding with HITT (Supplemental Figure 5B). We further identified the most potential residues by analysis the top 10 RGS2-HITT (1080-1130 nt) models predicted by HDOCK(26). Seven RGS2 residues (W80, S81, Y92, R133, F194, Q196 and D197) were identified to be the most potentially sites in bridging their interaction, because they were predicted by these 10 models for at least 5 times, and with a root mean square deviation (RMSD) values less than 3Å (Supplemental Table 3). Then, each of these amino acids was substituted (W80F, S81T, Y92F, R133K, F194Y, Q196R and D197A), and the combined substitution was generated (W80FS81T and F194YQ196RD197A) when they are close or next to each other (Supplemental Figure 5C). The following RNA pull-down assay revealed that none of single substitution had impacts on the interaction between RGS2 and HITT (1080-1130 nt). However, their interaction was largely diminished by triple mutation at sites F194YQ196RD197A (lane 10, Figure 4G), suggesting that F194, Q196, and D197 forms the surface to interact with HITT. The direct interaction between RGS2 and HITT was verified using the proximity ligation (PLA) assay in cells transfected HITT, but not those transfected with RGS2 binding defective mutant, HITT-del(1080-1130 nt) (Figure 4H). Thus, HITT directly binds with RGS2 mainly at F194, Q196 and D197 via its (1080-1130 nt) fragment. The interaction may be essential for their regulation of PD-L1 (see below).

K175, R176 and S179 in RGS domain is required for *PD-L1-5*'-UTR binding

We next asked how the RGS2/HITT complex influences PD-L1 translation. To answer this question, we generated two luciferase reporter plasmids, namely *PD-L1-5*'-UTR and *3*'-UTR luciferase reporters (as shown in the diagram, Supplemental Figure 5D). Strikingly, *PD-L1-5*'-UTR, but not *PD-L1-3*'-UTR, luciferase reporter activity was decreased by HITT overexpression and increased by HITT KD (Supplemental Figure 5, E and F). RGS2 KD enhanced *PD-L1-5*'-UTR luciferase activity and

completely abolished the effect of HITT (Figure 5A), confirming that RGS2/HITT imparts their negative regulation of PD-L1 expression through the 5′-UTR.

We further explored how RGS2/HITT regulates *PD-L1-5*′-UTR-dependent PD-L1 expression. It has been proposed before that RGS2 inhibits protein translation by binding with eIF2Bε(16). However, this is unlikely for RGS2-regulated PD-L1 expression (Supplemental Figure 5G). Intriguingly, by using a CLIP assay and RNA pull-down assay, as indicated in Figure 4, A and D, we found that RGS2 not only served as a HITT binding protein as described above (Figure 4, B and E), but also associated with the *PD-L1-5*′-UTR both in living cells and in vitro (Figure 5, B and C). The extreme 5′-end (1-36 nt) in the *PD-L1-5*′-UTR is essential for RGS2 binding, because the 1-36 nt and 1-72 nt regions, but not (37-108 nt), in the *PD-L1-5*′-UTR were found to co-precipitate with RGS2 (Supplemental Figure 5H). We then generated four compensatory mutants spanning across (1-36 nt) *PD-L1-5*′-UTR, as depicted in Figure 5D. Intriguingly, when 28-36 nt were substituted with their compensatory sequences (MT4), *PD-L1-5*′-UTR (1-36 nt) lost its RGS2 binding ability (Figure 5D), suggesting that the intact (28-36 nt) is required for *PD-L1-5*′-UTR's interaction with RGS2. Consistently, PLA-positive RGS2/*PD-L1-5*′-UTR complexes, but not RGS2/*PD-L1-5*′-UTR (1-36 nt)-MT4 complexes, were detected in HeLa cells (Figure 5E).

We also mapped the key *PD-L1-5*′-UTR binding residues in RGS2. Similar to HITT, *PD-L1-5*′-UTR also bound to RGS2(80-212aa), as revealed by the in vitro RNA binding assay (Supplemental Figure 5I. Following the similar approaches as described in Figure 4G, we predicted a set of residues, D85, N149, K175, R176 and S179, that may mediate its binding with *PD-L1-5*′-UTR using HDOCK (Supplemental Figure 5J and Supplemental Table 3). We tested the binding ability of the single mutants at each of these sites or triple mutant K175RR176KS179T (Figure 5F) and found that K175RR176KS179T remarkably reduced its binding with *PD-L1-5*′-UTR. Therefore K175, R176, and S179 provide the major *PD-L1-5*′-UTR binding sites of RGS2 (lane 7, Figure 5F).

HITT forms an RNA–RNA duplex with the *PD-L1-5*′-UTR

The newly identified binding mechanisms of RGS2/HITT and RGS2/*PD-L1-5*′-UTR, and the

coordinated inhibitory effect of HITT and RGS2 on PD-L1 translation, inspired us to explore how HITT contributes to RGS2-regulated and 5′-UTR-dependent PD-L1 translation. To this end, we first compared the binding of RGS2/*PD-L1-5*′-UTR in cells with different expression levels of HITT. The results showed that IFN-γ elevated HITT expression, which was accompanied by increased RGS2/*PD-L1-5*′-UTR binding (Figure 6A and Supplemental Figure 4C), while inhibition of IFN-γ-induced HITT expression dramatically reduced RGS2/*PD-L1-5*′-UTR complex levels (Figure 6A). Arbitrarily, expression of HITT produced a similar effect as IFN-γ-mediated endogenous HITT overexpression (Figure 6A). These data suggest that HITT facilitates binding between RGS2 and *PD-L1-5*′-UTR.

We further explored how HITT fulfills such a task by testing whether it forms an RNA–RNA complex with *PD-L1-5*′-UTR. In this RNA–RNA binding assay(27), we found that in vitro-synthesised HITT (unlabeled) was associated with Biotin-labeled-*PD-L1-5*′-UTR, but not Biotin-labeled-antisense *PD-L1-5*′-UTR (Figure 6, B and C). Remarkably, HITT antisense RNA disrupted the binding between HITT and *PD-L1-5*′-UTR (Supplemental Figure 6A). In addition, their binding was completely abrogated by RNase III or RNase A, but not RNase H (Figure 6C), suggesting the double-stranded RNA (HITT/PD-L1-5′-UTR) is formed. Furthermore, the colonization of HITT/*PD-L1-5*′-UTR was detected by fluorescence in situ hybridization (FISH) using Cy3-labeled-HITT probe and FAM-labeled-PD-L1-5′-UTR probe in cells under both basal and IFN-γ treated conditions (Figure 6D).

The RNA–RNA binding assay also revealed that HITT F3 (1030-2050 nt) and F3-1 (1030-1247 nt), but not other mutant fragments, contributed to *PD-L1-5*′-UTR binding (Figure 6C). The binding motif between F3-1 (1030-1247 nt) and *PD-L1-5*′-UTR was further analysed using a RNA–RNA interaction bioinformatic tool, IntaRNA. The highest-potential binding site between two RNA molecules was predicted to be 83-89 nt (binding site 1, BS1) and 97-105 nt (BS2) in *PD-L1-5*′-UTR (Figure 6E). To validate this bioinformatic result, point mutations on the *PD-L1-5*′-UTR that aimed to disrupt the RNA–RNA duplex were synthesised as shown in Figure 6E. No binding was detected between HITT and the Biotin-labeled-BS2-MT and BS1+2-MT *PD-L1-5*′-UTRs in the in vitro binding

assay (Figure 6F). Whereas WT and BS1-MT *PD-L1-5*'-UTRs, both of which retained the ability to bind with HITT, were found to dramatically improve RGS2's binding with the streptavidin magnetic beads to pull down Biotin-HITT. However, the BS2-MT and BS1+2-MT PD-L1-5'-UTRs, the two HITT binding-defective mutants, failed to do so (Figure 6G). Neither BS1 nor BS2 influenced *PD-L1-5*'-UTR's binding with RGS2 (Supplemental Figure 6B), which is consistent with above data showing that (1-36 nt) is essential for *PD-L1-5*'-UTR/RGS2 binding (Supplemental Figure 5H). In addition, HITT strengthened the binding between RGS2 and PD-L1-5'-UTR-WT or BS1-MT, but not the binding between RGS2 and PD-L1-5'-UTR-BS2-MT or BS1+2-MT (Supplemental Figure 6B). Taken together, HITT bridges and strengthens the interaction of *PD-L1-5*'-UTR with RGS2 by direct interaction with both *PD-L1-5*'-UTR at BS2 (Supplemental Figure 6C).

HITT/*PD-L1-5*'-UTR/RGS2 interactions are essential for PD-L1 inhibition

To validate a model where three molecules interact to inhibit PD-L1 translation, anti-Biotin-conjugated beads were used to pull-down Biotin-labeled-PD-L1-5'-UTR and its possible binding partners in the mixture. As shown, co-precipitated HITT was gradually increased with rising dose of Digoxin-labeled-HITT in the mixture (Figure 7A). Intriguingly, despite the same amount of RGS2 protein in the mixture, its binding with PD-L1-5'-UTR was also gradually increased with rising dose of HITT (lanes 1-3, Figure 7A). Therefore, the increased HITT not only enhances its own binding with PD-L1-5'-UTR, but also facilitates the binding of RGS2 with PD-L1-5'-UTR, suggesting the three molecules form one complex. We also found that HITT lost its ability to improve the binding between PD-L1-5'-UTR and PD-L1-5'-UTR binding deficient RGS2 (K175RR176KS179T) (lane 4, Figure 7A), suggesting that HITT recruits RGS2 to the complex and also promotes the direct binding between RGS2 to PD-L1-5'-UTR (Supplemental Figure 6C).

We then tested the essential roles of their interaction in regulating PD-L1 expression. Firstly, the impacts of the bindings of RGS2 with HITT or PD-L1-5'-UTR were tested after overexpression RGS2 wild type, RNA binding defective mutants (M2, K175RR176KS179T and M2, 194YQ196RD197A), and the combined mutant (M3, K175RR176KS179T-194YQ196RD197A) in HeLa cells. The

expression of PD-L1 was examined by WB. The HITT or PD-L1-5'-UTR binding defective mutants repressed PD-L1 expression, despite with a relative low efficiency when compared with wild type RGS2 (lanes 1-4, Supplemental Figure 6D). Whereas the combined substitution of all six amino acids completely abolished RGS2's ability to inhibit PD-L1 (lane 5, Supplemental Figure 6D). These data suggest that both bindings (RGS2/HITT and RGS2/PD-L1-5'-UTR) are essential for RGS2-mediated PD-L1 inhibition.

Secondly, the essential roles of HITT-mediated RGS2 binding were validated by another assay. As shown in Figure 7B, the fragments containing (1080-1130 nt) HITT, such as full-length HITT, F3-1, F3-1.1 and F3-1.2, were able to inhibit PD-L1 expression (lanes 2-5, Figure 7B). The other fragments (F3-1.3 and F3-1.4) failed to do so (lanes 6, 7, Figure 7B), further suggesting that the physical interaction between HITT and RGS2 is required for HITT-regulated PD-L1 inhibition.

Thirdly, using luciferase reporter assays, we found that RGS2 binding defective mutant PD-L1-5'-UTR-MT4 (compensatory mutation at 28-36 nt), but not other mutant reporter failed to response to RGS2 overexpression (Figure 7C), which provide additional evidence that RGS2/PD-L1-5'-UTR binding is essential for RGS2-mediated PD-L1 inhibition.

Fourthly, the critical roles of HITT/PD-L1-5'-UTR interactions in regulating PD-L1 expression were also examined. We found that HITT inhibited the activities PD-L1-5'-UTR luciferase reporters with the intact HITT binding site (BS2), such as WT and PD-L1-5'-UTR-BS1-MT reporter, and failed to change the luciferase reporter activities of PD-L1-5'-UTR-BS2-MT or BS1+2-MT (Figure 7D). These data suggest that the intact HITT binding site BS2 is necessary for HITT-mediated PD-L1 inhibition. Taken together, the three-way interaction among HITT/PD-L1-5'-UTR/RGS2 is critical for the inhibition of PD-L1 translation.

HITT inhibits T cell immunity in a PD-L1-dependent manner

Given the essential role of HITT in inhibiting PD-L1 expression, we compared the killing effects of CTLs before and after blocking PD-L1 signalling via anti-PD-1 antibody in foreign antigen chicken ovalbumin (OVA) expressing 4T1 cells (4T1-OVA). We consistently detected an increased killing

effect of OT-I T cells after co-culture with HITT overexpressing 4T1-OVA cells (Figure 8A). Anti-PD-1 antibody increased the killing effect of CTLs, as reported previously(28). The HITT-regulated CTL killing effect was completely abrogated by blocking PD-L1 signaling (Figure 8A). Consistently, a similar effect of HITT on the killing effect of human CTLs after co-culture with HITT overexpressing MDA-231 and HeLa cells was observed (Figure 8B and Supplemental Figure 7, A and B). Anti-PD-1 antibody or PD-L1 KD increased the killing effect of CTLs. The HITT-regulated CTL killing effect was completely abrogated by blocking PD-L1 signalling (Figure 8, B and C and Supplemental Figure 7, A and B). By contrast, PD-L1 over-expression repressed CTL-mediated cancer cell killing effects, and it also abolished HITT-induced killing effect of CTL (Supplemental Figure 7C). In line with these data, HITT lost its ability to regulate expression levels of IL-2 and IFN-γ after anti-PD-1 treatment (Supplemental Figure 7D). These data demonstrate that HITT mainly regulates T cell immunity by suppressing PD-L1 expression. Consistently, HITT KD increased the binding of PD-1 protein to the surfaces of cancer cells, as shown in a PD-1 binding assay (Figure 8D). Thus, HITT significantly enhances T cell cytotoxicity by inhibiting PD-L1 expression in cancer cells, leading to reduced interaction between PD-L1 and PD-1.

HITT inhibits tumour growth in vivo by preventing PD-L1-mediated T cell deactivation

We next explored whether HITT promotes T cell immunity in vivo using the 4T1/immune-competent BALB/c orthotopic model of murine mammary carcinoma. HITT-overexpressing orthotopic tumours grew relatively slow compared with control tumours (Figure 9, A-C). Anti-PD-1 antibody dramatically suppressed tumour growth compared with the correspond controls. Intriguingly, the effect of HITT was compromised, but not completely abolished, by anti-PD-1 (Figure 9, A-C). Above data were validated using HITT-expressing lentivirus administration in PD-L1 KO tumors (Supplemental Figure 8A-C and Supplemental Figure 8D-F). In contrast to HITT, PD-L1 5’-UTR binding defective HITT mutant (HITT-Mut) elicited little anti-tumor effect. Such sticking difference was completely abolished by PD-L1 KD (Supplemental Figure 8D-F). HITT-overexpression 4T1 tumour-bearing mice and anti-PD-1-treated mice survived significantly longer compared with

control 4T1 tumour-bearing mice treated with IgG control (Figure 9D). Anti-PD-1-treated HITT overexpressing 4T1 tumour-bearing mice survived longest among the four groups (Figure 9D). These data suggest that blocking PD-L1-mediated T cell inactivation by either anti-PD-1 antibody and/or HITT increases the survival of mammary tumour-bearing mice by suppressing tumour growth with low toxicity (Figure 9E).

Furthermore, HITT inhibited PD-L1 expression in orthotopic 4T1 tumours (Figure 9F and Supplemental Figure 8G-H). In addition, a significant increase of the activated tumour-infiltrated $CD8^+$ T cell population ($CD3^+CD8^+IFN\text{-}\gamma^+$) was detected in HITT-overexpressing tumours (Figure 9G). Anti-PD-1 antibody had no obvious effects on HITT or PD-L1 expression (Figure 9H), while treatment led to a significant increase in the activated tumour-infiltrated $CD8^+$ T cell population (Figure 9G). Anti-PD-1 antibody failed to further enhance the tumour-infiltrated $CD8^+$ T cell population in HITT-overexpressing 4T1 tumours (Figure 9G). Unlike the $CD8^+$ T cell population, tumour growth and mouse survival were both further decreased or prolonged by the combination of anti-PD-1 and HITT overexpression (Figure 9, A-C).

The association between HITT/RGS2 and PD-L1 in breast cancer tissues

qRT-PCR assay revealed that HITT was downregulated in breast cancer tissues compared with the adjacent normal controls (Figure 10A), while PD-L1 protein levels were increased in breast cancer tissues, as indicated by WB assays (Figure 10, B and C). The decreased HITT and increased PD-L1 were both associated the advanced stages of breast cancers (Figure 10, D and E). In addition, a negative association between the fold change of HITT and those of PD-L1 protein was detected (Figure 10F). RGS2 was also found to be decreased in breast cancer tissues and its downregulation was more evident in the advanced breast cancers (Figure 10, B and G and H). Similar to HITT, RGS2 fold change exhibited a negative correlation with PD-L1 protein fold change (Figure 10I). Neither HITT nor RGS2 correlated with the mRNA levels of PD-L1 (Figure 10, J and K). Therefore, RGS2/HITT may contribute to PD-L1 regulation in vivo in human cancer tissues.

Discussion

Here, we describe a novel mechanism that regulates PD-L1 translation: an IFN-γ-responsive lncRNA called HITT that, in coordination with RGS2, binds the *PD-L1-5*'-UTR resulting in reduced mRNA translation, as indicated by the decreased occupancy of *PD-L1* mRNA by polysomes and reduced *de novo* protein synthesis. In addition, arbitrarily increasing HITT expression in cancer cells promotes T cell-mediated cancer killing effects by inhibiting the PD-1/PD-L1 axis both in vitro and in vivo. Furthermore, a negative association between HITT/RGS2 and PD-L1 expression was detected in vivo in human breast cancers, suggesting that HITT may inhibit PD-L1 expression in vivo (Figure 10L). Thus, translational suppression of PD-L1 expression by HITT/RGS2 may represent an alternative strategy against cancer and a novel marker for prediction of the anti-PD-1/PD-L1 response.

Previous studies have indicated that constitutive expression of PD-L1 on cancer cells, despite it having a defined role in tumourigenesis, is less reliable than inflammation-induced PD-L1 expression for the prediction of response to immunotherapy(25). In terms of anti-PD-1/PD-L1 therapies, it is essential that we understand the regulatory mechanism behind IFN-γ-increased PD-L1 expression. Interestingly, HITT is activated by IFN-γ in the microenvironment. Although inflammation simultaneously elevates PD-L1 and HITT expression, HITT significantly relieves PD-L1 elevation induced by IFN-γ. These data suggest that IFN-γ-induced pro- and anti-immunity factors are interconnected and regulate overall functional output of IFN-γ. Moreover, HITT restrains PD-L1 expression in a variety of cancer types, suggesting that HITT's inhibition of PD-L1 expression is a broad mechanism. Considering the ability of HITT to respond to IFN-γ signals and the improved response of HITT-overexpressing cancer cells or tumours to anti-PD-1 treatment, it is worth investigating whether HITT can predict response to anti-PD-1/PD-L1 treatment in future studies. In addition, HITT is sensitive to diverse cancer-related stimuli and its activity is regulated by several different mechanisms (22, 23). Here, we found that E2F1, but not EGR1, is required for the transcriptional activation of HITT upon IFN-γ stimulation. This finding is consistent with the notion that E2F1 is a transcription factor that is important in the inflammatory response(29). Whether or

not EGR1 activation upon other inflammatory signals contributes to the activation of HITT and subsequent immune surveillance needs to be investigated in future.

Notably, although HITT overexpression and an anti-PD-1 monoclonal antibody have similar effects on T cell activity, their combination leads to a synergetic effect that inhibits tumour growth and prolongs the survival of mice bearing 4T1 tumours. Given the remarkable effect of HITT on T cell activity and the synergetic effect observed in combination with anti-PD-1 antibody therapy, it would be worth evaluating the therapeutic potential of the lncRNA HITT.

In addition, although mechanisms of PD-L1 regulation have not been fully investigated, recent studies suggest that cancer cells utilise comprehensive mechanisms to fine-tune PD-L1 expression. For example, STAT3, C-Myc, HIF-1α, c-JUN and NF-κB increase PD-L1 expression at the transcriptional level. CSN5, GSK3β, CDK4/CDK6, CMTM4/6, and B3GNT have been shown to regulate PD-L1 degradation(30). Connection between PD-L1 expression and lncRNAs has also been suggested. Some lncRNAs were found to regulate PD-L1 mRNA levels by targeting microRNAs. Recently, Mineo et al. reported that lncRNA *INCR1* is activated in response to IFN-γ and promotes PD-L1 transcription *in cis* by binding with *HNRNPH1*(31). Another lncRNA, *lncMX1–215*, is induced by IFN-γ and regulates PD-L1 transcription via an epigenetic mechanism(32). For the first time, a lncRNA (HITT) has been shown to directly connect with PD-L1 translation. In support of our data, Suresh et al. and Xu et al. have demonstrated the essential contribution of *PD-L1* mRNA translation in controlling its expression (33, 34). Of note, although alterations in translation normally lead to mRNA degradation(35), there are a few exceptions. HITT inhibits PD-L1 translation, while had no obvious impacts on its mRNA levels, which provides another example of the independent regulation of translation and mRNA stabilization. These data, together with our findings in this study, are coherent with the emerging idea that translation is an efficient mechanism that dynamically controls protein abundance with the advantage of promoting a response.

Mechanistically, our results demonstrate that HITT's reduction of PD-L1 translation relies on the inhibition of cap-dependent initiation. However, BS2-mediated HITT/PD-L1-5'-UTR interaction is

required, but not sufficient for the optimal inhibition of PD-L1. Based on the features of HITT in activating T cell immunity and in inhibiting PD-L1 translation, proteins possibly involved in this process was screened in the GO database followed by literature search. Interestingly, among such proteins, RGS2 is uniquely required for HITT-inhibited PD-L1 translation. Notably, RGS2 is reported to bind with eIF2Bε to fulfil its role in regulating mRNA translation, yet RGS2 inhibits PD-L1 expression in eIF2Bε KD cells, which implies that RGS2 has a novel translation regulatory mechanism(16). Indeed, for the first time, we reported an RNA-binding activity of RGS2, which is required for inhibition of PD-L1 translation. HITT/RGS2 regulates PD-L1 translation in a *PD-L1-5*'-UTR-dependent manner. HITT, RGS2, and *PD-L1-5*'-UTR interact with each other. HITT and RGS2 are interdependent in regulating PD-L1-5'-UTR reporter activity and PD-L1 translation. Based on these results, we propose a model that pairwise interaction of HITT/RGS2/*PD-L1-5*'-UTR is essential for impairing PD-L1 translation under both basal and IFN-γ-stimulated conditions. This model was further validated by examining PD-L1 expression or *PD-L1-5*'-UTR luciferase activity using binding-defective RGS2, HITT, or *PD-L1-5*'-UTR mutants, as shown in Figure 7. The multiple factors involved regulation allows precise and selective control of PD-L1 expression. It should be also noted that lncRNA is normally very low abundance. Thus, the question arising from the data presented is how to reconcile the low abundance of HITT with its apparent functional importance by interacting with PD-L1 mRNA. Whether HITT is concentrated by phase separation warrant further investigation. In addition, HITT may initiate the inhibitory reaction on PD-L1 expression. This may be followed by translational inhibition mediated by additional unknown factors, which may amplify the inhibitory signal to PD-L1 translation even when HITT is release from the PD-L1-5'-UTR complex. This model is also worthy of further exploration.

In support of a role for RGS2 in regulating T cell immunity, a previous report has shown that *rgs2*$^{-/-}$ mice have abnormal T cell immunity, which the authors propose may be due to increased cAMP levels in T cells mediated by loss of RGS2(17). To date, RGS2 has only been implicated in the regulation of T cell activity. In our study, we demonstrate for the first time the activity and

mechanism by which RGS2 expression in cancer cells regulates immune surveillance.

Moreover, in agreement with the finding that increased PD-L1 expression is associated with poor outcomes of breast cancer patients, our data also reveal the predictive value of PD-L1. Oncogene signals, such as Myc overexpression, Ras activation, loss of PTEN, or PI3K/Akt mutation, contribute to the constitutive activation of PD-L1 in cancer cells(30). Our data provide an alternative explanation for PD-L1 dysregulation, because the decreased expression of HITT is inversely correlated with PD-L1 expression in breast cancer tissues, and the inhibitory activity of HITT on PD-L1 expression can be demonstrated both in vitro and in orthotopic models.

Together, our data elucidate a distinctive mechanism by which PD-L1 expression is regulated and uncover novel antitumour activity of HITT and RGS2 through the prevention of tumour cell immune escape. Our research provides new insight into the network that regulates immunosuppression and may enhance the antitumour effects of immune checkpoint blockade therapies.

Methods

Human breast cancer tissues

For human breast cancer tissues and their corresponding adjacent normal controls were collected from Qilu Hospital of Shandong University in China. Written informed consent was obtained from all patients. The study has been approved by the Research Ethics Committee of Shandong University, China. Specimens were collected and stored in liquid nitrogen immediately after surgery.

Animal experiments.

BALB/c mice (6 week-old females) were purchased from Beijing HFK Bioscience Co., Ltd. Mice were randomly divided into four groups. 50,000 4T1 cells in 100μL 1×PBS were injected into the mammary fat fad. To block PD-L1/PD-1 signaling, 100μg anti-PD-1 antibody was injected intraperitoneally into mice at 3, 6, and 9 days post-tumour inoculation, with IgG as a negative control(36). To block CD8 T cell function, three days after tumour inoculation, 20μg of monoclonal anti-CD8α antibody were administered via intraperitoneal injection every other day for three weeks(37). For the HITT-expressing lentivirus anti-tumor treatments, mice bearing similar size of tumor (80mm^3) were randomly divided into five groups: 1) PBS, 2) Lenti-Vect+IgG, 3) lenti-HITT+IgG, 4) Lenti-Vect+anti-PD-1 antibody, 5) lenti-HITT+anti-PD-1 antibody. PBS alone, Lentiviruses (1×10^8 pfu) and IgG or anti-PD-1 antibody (100μg) in 100μl 1×PBS were administered intratumorally at three sites per tumor. The treatments were repeated every 2 days for 4 times. Tumour volume were measured every 3 days with a caliper using the following formula: $\pi/6 \times \text{length} \times \text{width}^2$(38). At the end point, the tumour was carefully peeled, photographed, weighed. Protein, RNA and T cells were collected for the further analysis.

Cell culture, stable transfectants and transfection

The human breast cancer (MDA-231, MDA-453, MDA-468, BT549, BT474, MCF7, T47D), colorectal

cancer (HT29), cervical cancer (HeLa) cells, lung cancer (H23, H1299) and the mouse breast cancer (4T1) cells were purchased from the American Type Culture Collection and cultured in RPMI-1640 medium (Gibco, Carlsbad, CA, USA) or Dulbecco's modified Eagle's medium supplemented with 10% (v/v) FBS (Biological industries). All cells were cultured in the humidified incubator at 37°C under 5% CO_2. Stable cell lines overexpressing HITT and the vector control were established as previously described. For the transient transfection, the indicated plasmid constructs or siRNAs were introduced into cells with Lipofectamine 2000 (Life Technologies, Carlsbad, CA, USA) according to the manufacturer's instruction. 48-72h after transfection, the cells were subjected to the indicated treatments or analysis. For IFN-γ treatment, cells were serum starved overnight prior to stimulation at the indicated time periods or concentrations. The plasmids used in this study were listed in Supplemental Table 4.

Lentivirus production

HITT were inserted into the lentivirus vector pLnc-KP. The 3,000ng pLnc-KP control or recombined pLnc-KP-HITT were transfected respectively into 293T cells with 1,500ng pGag/pol, 900ng pVSVG, and 600ng pRev lentiviral packing vectors using Lipofectamine 2,000 according to the manufacturer's instructions. 48h after transfection, the supernatant was collected and centrifuged at 4,000g for 10min and then filtrated with 0.45nm filter to harvest the lentivirus particles.

T cell-mediated tumour cell-killing assay

The assay was performed according to previous report(25, 39). Briefly, human peripheral blood mononuclear cells (PBMC) obtained from 3 differant healthy donors from Harbin Blood Institute, which were maintained in F12-K medium supplemented with 10% FBS. T cells were activated by treating PBMC with anti-CD3 antibody (100ng/ml), anti-CD28 antibody (100ng/ml) and IL-2 (10ng/ml) for 48h(40, 41). 5×10^5 of cancer cells were seeded in a 24-well plate. 24h later, $5x10^6$ activated T cells (10:1) were seeded and co-cultured with the indicated cancer cells for additional 6h. Then, cells were washed twice with 1×PBS to discard T cells and suspended dead cancer cells. The remaining living cells were fixed with 4% formaldehyde for 30min at room temperature, and

stained with 0.1% crystal violet solution for 20min. After four times washes with 1×PBS, the plates were photographed and quantified. Alternatively, T cell cytotoxicity activity can also be determined using MTS reagent kit following the manufacturers' introduction (CellTiter 96 AQueous One Solution Cell, Promega).

OT-I T cell-based tumour killing assay was performed as described previously(25). C57BL/6-Tg (TcraTcrb) 1100Mjb/J (OT-I) mice were purchased from Shanghai Model Organisms Center, lnc. The mice express T-cell receptor recognizing an H-2b-restricted OVA 257-264 epitope, SIINFEKL. For OT-I T cell isolation, the spleen was homogenized and the single splenocytes were pelleted and suspended in red blood cell lysis buffer (NH_4CL, 0.15M; $KHCO_3$, 10mM; Na_2EDTA, 0.1mM). Then splenocytes were resuspended at the density of 2×10^6/ml in RPMI culture medium containing 1μg/ml OVA 257-264 peptide, 5μg/ml mouse recombinant IL-2 and 40μM 2-mercaptoethanol. OT-I T cells were isolated and purified by mouse CD8+ T cell MicroBeads (Miltenyi Biotec) after incubation at 37°C for 5 days. The FACS assay confirmed that over 90% were CD8+ T cell. OVA expressing 4T1 cells were established by introducing OVA into 4T1 cells (4T1-OVA), which were seeded overnight. OT-I T cells were added into the culture (4T1-OVA: OT-I T, 1:4). The OT-I T cell-mediated 4T1-OVA cell-killing effect was evaluated by crystal violet staining 48 h after addition of T cells. The images were quantified by Image J software (1.52a).

Enzyme-Linked Immunosorbent Assay (ELISA) of IL-2 and IFN-γ.

20,000 cancer cells were seeded in 96-well plates. The cancer cells and T cells were washed with 1×PBS to eradicate contaminating traces of IFN-γ or IL-2 in the culture medium. 10,000 activated T cells were incubated with the cancer cells in 96-well plates for additional 72h. 10μg/ml of anti-PD-1 antibody or IgG control were added in the co-culture system where indicated. 100μl of 200μl total supernatant was subjected to the measure of the secreted IL-2 and IFN-γ protein using IL-2/IFN-γ kits (Human Quantikine IL-2/IFN-γ ELISA Kits R&D Systems) according to the manufacture's introduction. Each experiment was repeated three times.

Quantitative reverse transcription PCR (qRT-PCR) assay

554 Cells were washed twice with 1×phosphate-buffered saline (PBS) and then total RNA was extracted
555 using Trizol Reagent (Takara). 2μg purified RNA was used to synthesise cDNA according with the
556 manufacture's protocol (Prime Script ^{TM} RT reagent Kit with gDNA Eraser). qPCR was performed in
557 triplicate with the ViiA7 real-time PCR instrument (Applied Biosystems) using SYBR Premix Ex Taq
558 II kit (RR820L; Takara). Relative expression levels of the targeted genes compared with the *18S*
559 *rRNA* or *GAPDH* were calculated using $2^{-\Delta\Delta CT}$ method. The primer sequences used in RT-PCR were
560 listed in Supplemental Table 5.

561 **Western blot (WB) assay**

562 Cells or tissue samples were lysed with UREA buffer (8M Urea, 1M Thiourea, 0.5% CHAPS, 50mM
563 DTT, and 24mM Spermine) and fully vibrate for 30min at room temperature. Same amount of
564 proteins were separated by sodium dodecyl sulfate-polyacrylamide gel electrophoresis (SDS-PAGE).
565 After transferring, PVDF membrane with proteins were incubated with the indicated primary
566 antibodies and the secondary antibodies, the protein signals were visualised by ECL (32106,
567 Thermo Scientific) and the images were captured by Image studio system (ECL, LI-COR, Lincoln,
568 Georgia, USA). The antibodies are listed in Supplemental Table 6.

569 **Luciferase reporter assay**

570 Luciferase reporter gene expression plasmids and the Renilla-luciferase control plasmid were
571 transfected into cells. 48h after transfection, cells were harvested using luciferase lysis buffer and
572 subjected to analysis of the Dual Luciferase Reporter Assay according to the manufacture's
573 protocols (Promega, #E1910). The luciferase reporter activities were determined as the ratio of the
574 target gene luciferase to the Renilla-luciferase control.

575 **Chromatin immunoprecipitation (ChIP)**

576 Briefly, cells were pre-treated with 1% formaldehyde in the culture media for 20min at 37°C to yield
577 protein-DNA cross-link complexes and then the complexes were extracted and sonicated in the
578 ChIP lysis buffer. The purified chromatin was equally separated and incubated with either anti-E2F1
579 antibody or IgG control overnight at 4°C. Thereafter, the immunoprecipitates were collected by

centrifugation and the resulting protein-DNA complexes were de-crosslinked at 65°C. After four times washes in 1×PBS, the the fragmented DNA was extracted by the Axygen product purification kit and subjected to PCR analysis.

L-azidohomoalanine labelling to identify newly synthesized proteins

MDA-231 cells were washed three times in 1×PBS and then incubated in methionine-free medium for 30min to wipe off residual methionine. Then, cells were incubated with 50μM L-azidohomoalanine (AHA, Invitrogen, Carlsbad, CA, USA) at 37°C for 4h. After the treatments, cells were sonicated followed by a centrifuge at 13,000g for 30min. 50mg of resulting supernatant were subjected to the treatment with Click reactions (Click-iT® Protein Reaction Buffer Kit; Invitrogen, Carlsbad, CA, USA). Total proteins from Click reactions were pelleted by centrifugation in the presence of methanol/chloroform and the resolubilised proteins were incubated with 50μl of Streptavidin coupled magnetic beads for 5h at room temperature. Proteins linked with magnetic beads were boiled in 30μl 5×loading buffer for 10min at 100°C and then subjected to WB analysis.

Polysome Profiling

3×10^7 cells were treated with 0.1mg/ml cycloheximide (CHX) for 5min, before lysing in polysome lysis buffer (15mM Tris-HCL PH 7.5, 15mM $MgCl_2$, 0.3M NaCl, 1% Triton X-100, 0.1U/μl RNA inhibitor, 100μg/ml CHX, 1μg/ml Heparin, and 1×protease inhibitor cocktail). Nuclei and membrane debris was removed by centrifuging at 10,000g, for 5min and lysate was loaded across sucrose gradients. The sucrose gradient samples were obtained by centrifuge at 39,000 rpm for 2h at 4°C using SW40Ti rotor in a Beckman Coulter and fractionated RNA samples were monitored by using ultraviolet spectrophotometer at 254nm. RNA in each sucrose gradient was collected and extracted in 3 volumes of Trizol, followed by qRT-PCR assay for the indicated gene.

UV-cross-linking RNA-IP (CLIP)

Cells were washed twice in 1×PBS and then subjected to UV cross-linking at 400mJ/cm^2. The UV cross-linked cells were lyzed in the lysis buffer (50mM Tris-HCl [pH 8.1], 85mM KCl, 10mM EDTA, 5mM PIPES [pH 8.0], 1% SDS and 0.5% NP40) supplemented with Protease Inhibitor Cocktail and

RNase inhibitor (Thermo Fisher, Rockford, IL). Total lysates were pre-cleaned by protein G sepharose beads at 4°C for 1h. The supernatant was collected and incubated with the indicated primary antibodies or IgG control, rotating at 4°C overnight. The next day, the antibody-RNA complexes were collected and incubated with the blocked protein A/G sepharose beads for 1h. After that, the immunoprecipitated RNA was eluted, isolated and reverse transcribed to cDNA for the subsequent qRT-PCR analysis.

In vitro RNA pull-down assay

Biotin-labeled RNA was synthesized in vitro using Biotin RNA Labeling Mix (Roche, St Louis, MO, USA, 11685597910). After treatment with RNase-free DNase I, Biotin-labeled RNA was heated at 95°C for 2min followed by 3min's incubation on ice to recover the secondary structure of RNA. The RNA was then incubated with streptavidin agarose beads (Invitrogen, Carlsbad, CA, USA) overnight. The fresh cell lysates were collected and added to RNA-captured beads and the mixture was incubated at 4°C for 1h. After four times washes in 1×PBS, the beads were boiled at 95°C for 5min in SDS loading buffer and the associated proteins were detected by WB assay.

PD-1/PD-L1 interaction assay

Briefly, 72h after HITT KD, MDA-231 cells were washed twice in 1×PBS and fixed with 4% paraformaldehyde for 20min at room temperature. Cells were incubated with 5μg/ml recombinant human PD-1 Fc protein at 4°C overnight, followed by additional incubation with the anti-human Alexa Fluor 488 dye-conjugated secondary antibody for 30min at room temperature. Then nuclei were stained with DAPI at room temperature for 5min. After incubation with PD-1 Fc protein, the following process was protected from exposure to light. Images were acquired by a Zeiss confocal microscope (LSM880, Germany) after counterstained with DAPI at room temperatures for 5min.

Proximity ligation assay (PLA)

Cells grown on cover slips were permeabilized with 1% saponin (w/v) for 1h at room temperature, followed by blocking with blocking buffer (10mM Tris-acetate, pH 7.5, 10mM magnesium acetate, 50mM potassium acetate, 250mM NaCl, 0.25μg/μL bovine serum albumin [BSA], and 0.05% Tween

20) in the presence of 20μg/mL sheared salmon sperm DNA (sssDNA) at 4°C for 1h. 100nM specific RNA probes were added to fresh blocking buffer, heated at 70°C for 3min, and incubated with fixed/permeabilized cells at 37°C for 1h. Subsequently, the cells were blocked in 1×PBS with 0.1% Tween 20 containing 1% (v/v) BSA and 20μg/mL sssDNA at room temperature for 1h. After that, cells were incubated with anti-RGS2 and anti-Biotin antibodies derived from different species at 4°C overnight at a dilution rate of 1:50. The subsequent PLA ligation and amplification steps were performed according to the manufacturer's instructions. (Duolink in situ PLA kit, Duo92004; Duo92002; Duo92008; Sigma). The probe sequences used in PLA were listed in Supplemental Table 7.

Fluorescence in situ hybridization (FISH)

FISH was performed by following the manufacture's introduction (Gene Pharma). Briefly, after IFN-γ stimulation, HeLa cells were fixed in 4% PFA solution at room temperature for 15min. The cells were treated with 0.1% Buffer A (0.1% Triton X-100) at room temperature for 15min followed by another round of incubation in Buffer C (2×SSC) at 37°C for 30min. Then slide was incubated with denaturated FAM-labeled PD-L1-5'-UTR and Cy3-labeled-HITT probes (8μM final concentration) in Buffer E (1×SSC, 35% formamide, 10% dextran sulfate) at 37°C overnight and then washed sequentially with Buffer F (0.1% Tween 20) and Buffer C at 42°C for 5min each. Finally, images were acquired by a Zeiss confocal microscope (LSM880, Germany) after counterstained with DAPI at room temperatures for 5min. The probes sequences used in FISH assays were listed in Supplemental Table 7.

Tumour infiltration lymphocyte analysis

Tumour infiltration lymphocyte profile analysis was conducted as described previously. Briefly, 4T1 syngeneic tumors dissected from mice were digested in collagenase/hyalurinidase (Stemcell Technologies, Vancouver, BC, Canada) and DNase (Sigma), and T cells were enriched sequentially on a Ficoll gradient (Sigma) and Dynabeads untouched mouse T cell kit (Invitrogen). The isolated T cells were fixed with 4% paraformaldehyde for 5min and stained with PE-CD3ε (145-2C11;

Biolegend), PE-Cyanine7-IFN-γ (XMG1.2; Biolegend), and FITC-CD8a (53-6.7; BD Pharmingen™) for 30min at room temperature. After three times washed, the populations of infiltration T cells were detected and analysed with BD FACS (LSRF Fottessa) cytometer.

Data availability

Mass-spectrum data have been deposited to the ProteomeXchange Consortium via the iProX partner repository with the dataset identifier PXD039107.

Statistics

Data are presented as the means ± standard error of the means (SEM) or standard Deviation (SD). Statistical significance of differences between two groups was evaluated by 2-tailed Student's t test, while statistical significance of differences among multiple groups was analyzed by Analysis of Variance (ANOVA) using GraphPad Prism software. Correlations were calculated according to Pearson correlation. Significance of survival difference was determined by the log-rank test (n = 10 per group). *P* values less than 0.05 were considered statistically significant.

Study approval

The experiments with BALB/c mice were conducted according to protocols approved by the Rules for Animal Experiments published by the Chinese Government (Beijing, China) and approved by the Research Ethics Committee of Harbin Institute of Technology, China.

Author Contributions

H. designed and supervised the project and wrote the paper. Q.L., X.W., G.H., Z.X., W.Z., D.Z., M.L., and T. G. performed the experiments. Q.L., G.H., Z.X., S.Z., H.L. and D.Z. analyzed the data. Q.L. and Q. L. performed animal experiments. T.L. and S.Z. collected clinical breast cancer samples and analyzed clinical data.

Acknowledgments

The work was funded by National Key R&D Program of China (2022YFA1105200), National Nature Science Foundation (No. 82150115, 82025027 and 32000517), Interdisciplinary Research Foundation of HIT and China Postdoctoral Science Foundation (No. 2022TQ0093).

References

1. Palucka AK, and Coussens LM. The Basis of Oncoimmunology. *Cell.* 2016;164(6):1233-47.
2. Ribas A. Adaptive Immune Resistance: How Cancer Protects from Immune Attack. *Cancer Discov.* 2015;5(9):915-9.
3. Zou W, Wolchok JD, and Chen L. PD-L1 (B7-H1) and PD-1 pathway blockade for cancer therapy: Mechanisms, response biomarkers, and combinations. *Sci Transl Med.* 2016;8(328):328rv4.
4. Sun C, Mezzadra R, and Schumacher TN. Regulation and Function of the PD-L1 Checkpoint. *Immunity.* 2018;48(3):434-52.
5. Li Z, Wu X, Zhao Y, Xiao Y, Zhao Y, Zhang T, et al. Clinical benefit of neoadjuvant anti-PD-1/PD-L1 utilization among different tumors. *MedComm.* 2021;2(1):60-8.
6. Hegde PS, and Chen DS. Top 10 Challenges in Cancer Immunotherapy. *Immunity.* 2020;52(1):17-35.
7. Herbst RS, Soria JC, Kowanetz M, Fine GD, Hamid O, Gordon MS, et al. Predictive correlates of response to the anti-PD-L1 antibody MPDL3280A in cancer patients. *Nature.* 2014;515(7528):563-7.
8. Sharma P, Retz M, Siefker-Radtke A, Baron A, Necchi A, Bedke J, et al. Nivolumab in metastatic urothelial carcinoma after platinum therapy (CheckMate 275): a multicentre, single-arm, phase 2 trial. *Lancet Oncol.* 2017;18(3):312-22.
9. Klepac K, Yang J, Hildebrand S, and Pfeifer A. RGS2: A multifunctional signaling hub that balances brown adipose tissue function and differentiation. *Mol Metab.* 2019;30:173-83.
10. Tang KM, Wang GR, Lu P, Karas RH, Aronovitz M, Heximer SP, et al. Regulator of G-protein signaling-2 mediates vascular smooth muscle relaxation and blood pressure. *Nat Med.* 2003;9(12):1506-12.
11. Mark MD, Wollenweber P, Gesk A, Kösters K, Batzke K, Janoschka C, et al. RGS2 drives male aggression in mice via the serotonergic system. *Commun Biol.* 2019;2:373.
12. Phan HTN, Jackson WF, Shaw VS, Watts SW, and Neubig RR. Loss-of-Function Mutations in Human Regulator of G Protein Signaling RGS2 Differentially Regulate Pharmacological Reactivity of Resistance Vasculature. *Mol Pharmacol.* 2019;96(6):826-34.
13. Qin W, Cho KF, Cavanagh PE, and Ting AY. Deciphering molecular interactions by proximity labeling. *Nat Methods.* 2021;18(2):133-43.
14. Cho J, Min HY, Lee HJ, Hyun SY, Sim JY, Noh M, et al. RGS2-mediated translational control mediates cancer cell dormancy and tumor relapse. *J Clin Invest.* 2021;131(1):e136799.15.
15. Cacan E. Epigenetic regulation of RGS2 (Regulator of G-protein signaling 2) in chemoresistant ovarian cancer cells. *J Chemother.* 2017;29(3):173-8.
16. Nguyen CH, Ming H, Zhao P, Hugendubler L, Gros R, Kimball SR, et al. Translational control by RGS2. *J Cell Biol.* 2009;186(5):755-65.
17. Oliveira-Dos-Santos AJ, Matsumoto G, Snow BE, Bai D, Houston FP, Whishaw IQ, et al. Regulation of T cell activation, anxiety, and male aggression by RGS2. *Proc Natl Acad Sci U S A.* 2000;97(22):12272-7.
18. George T, Chakraborty M, Giembycz MA, and Newton R. A bronchoprotective role for Rgs2 in a murine model of lipopolysaccharide-induced airways inflammation. *Allergy Asthma Clin Immunol.* 2018;14:40.

19. Ulitsky I, and Bartel DP. lincRNAs: genomics, evolution, and mechanisms. *Cell.* 2013;154(1):26-46.
20. Mercer TR, Dinger ME, and Mattick JS. Long non-coding RNAs: insights into functions. *Nat Rev Genet.* 2009;10(3):155-9.
21. Schmitt AM, and Chang HY. Long Noncoding RNAs in Cancer Pathways. *Cancer Cell.* 2016;29(4):452-63.
22. Wang X, Li L, Zhao K, Lin Q, Li H, Xue X, et al. A novel LncRNA HITT forms a regulatory loop with HIF-1α to modulate angiogenesis and tumor growth. *Cell Death Differ.* 2020;27(4):1431-46.
23. Zhao K, Wang X, Xue X, Li L, and Hu Y. A long noncoding RNA sensitizes genotoxic treatment by attenuating ATM activation and homologous recombination repair in cancers. *PLoS Biol.* 2020;18(3):e3000666.
24. Wang TT, Zhao YL, Peng LS, Chen N, Chen W, Lv YP, et al. Tumour-activated neutrophils in gastric cancer foster immune suppression and disease progression through GM-CSF-PD-L1 pathway. *Gut.* 2017;66(11):1900-11.
25. Lim SO, Li CW, Xia W, Cha JH, Chan LC, Wu Y, et al. Deubiquitination and Stabilization of PD-L1 by CSN5. *Cancer Cell.* 2016;30(6):925-39.
26. Yan Y, Zhang D, Zhou P, Li B, and Huang SY. HDOCK: a web server for protein-protein and protein-DNA/RNA docking based on a hybrid strategy. *Nucleic Acids Res.* 2017;45(W1):W365-w73.
27. Cai Z, Cao C, Ji L, Ye R, Wang D, Xia C, et al. RIC-seq for global in situ profiling of RNA-RNA spatial interactions. *Nature.* 2020;582(7812):432-7.
28. Stein S, Henze L, Poch T, Carambia A, Krech T, Preti M, et al. IL-17A/F enable cholangiocytes to restrict T cell-driven experimental cholangitis by upregulating PD-L1 expression. *J Hepatol.* 2021;74(4):919-30.
29. Murata K, Fang C, Terao C, Giannopoulou EG, Lee YJ, Lee MJ, et al. Hypoxia-Sensitive COMMD1 Integrates Signaling and Cellular Metabolism in Human Macrophages and Suppresses Osteoclastogenesis. *Immunity.* 2017;47(1):66-79.e5.
30. Cha JH, Chan LC, Li CW, Hsu JL, and Hung MC. Mechanisms Controlling PD-L1 Expression in Cancer. *Mol Cell.* 2019;76(3):359-70.
31. Mineo M, Lyons SM, Zdioruk M, von Spreckelsen N, Ferrer-Luna R, Ito H, et al. Tumor Interferon Signaling Is Regulated by a lncRNA INCR1 Transcribed from the PD-L1 Locus. *Mol Cell.* 2020;78(6):1207-23.e8.
32. Ma H, Chang H, Yang W, Lu Y, Hu J, and Jin S. A novel IFNα-induced long noncoding RNA negatively regulates immunosuppression by interrupting H3K27 acetylation in head and neck squamous cell carcinoma. *Mol Cancer.* 2020;19(1):4.
33. Xu Y, Poggio M, Jin HY, Shi Z, Forester CM, Wang Y, et al. Translation control of the immune checkpoint in cancer and its therapeutic targeting. *Nat Med.*2019;25(2):301-11.
34. Suresh S, Chen B, Zhu J, Golden RJ, Lu C, Evers BM, et al. eIF5B drives integrated stress response-dependent translation of PD-L1 in lung cancer. *Nat Cancer.* 2020;1(5):533-45.
35. Jia L, Mao Y, Ji Q, Dersh D, Yewdell JW, and Qian SB. Decoding mRNA translatability and stability from the 5' UTR. *Natur Struct Mol Biol.* 2020;27(9):814-21.
36. Li CW, Lim SO, Xia W, Lee HH, Chan LC, Kuo CW, et al. Glycosylation and stabilization of

programmed death ligand-1 suppresses T-cell activity. *Nat Commun.* 2016;7:12632.
37. Gangoso E, Southgate B, Bradley L, Rus S, Galvez-Cancino F, McGivern N, et al. Glioblastomas acquire myeloid-affiliated transcriptional programs via epigenetic immunoediting to elicit immune evasion. *Cell.* 2021;184(9):2454-70.e26.
38. Tomayko MM, and Reynolds CP. Determination of subcutaneous tumor size in athymic (nude) mice. *Cancer Chemother Pharmacol.* 1989;24(3):148-54.
39. Burr ML, Sparbier CE, Chan YC, Williamson JC, Woods K, Beavis PA, et al. CMTM6 maintains the expression of PD-L1 and regulates anti-tumour immunity. *Nature.* 2017;549(7670):101-5.
40. Schneider E, Winzer R, Rissiek A, Ricklefs I, Meyer-Schwesinger C, Ricklefs FL, et al. CD73-mediated adenosine production by CD8 T cell-derived extracellular vesicles constitutes an intrinsic mechanism of immune suppression. *Nat Commun.* 2021;12(1):5911.
41. Legut M, Gajic Z, Guarino M, Daniloski Z, Rahman JA, Xue X, et al. A genome-scale screen for synthetic drivers of T cell proliferation. *Nature.* 2022;603(7902):728-35.

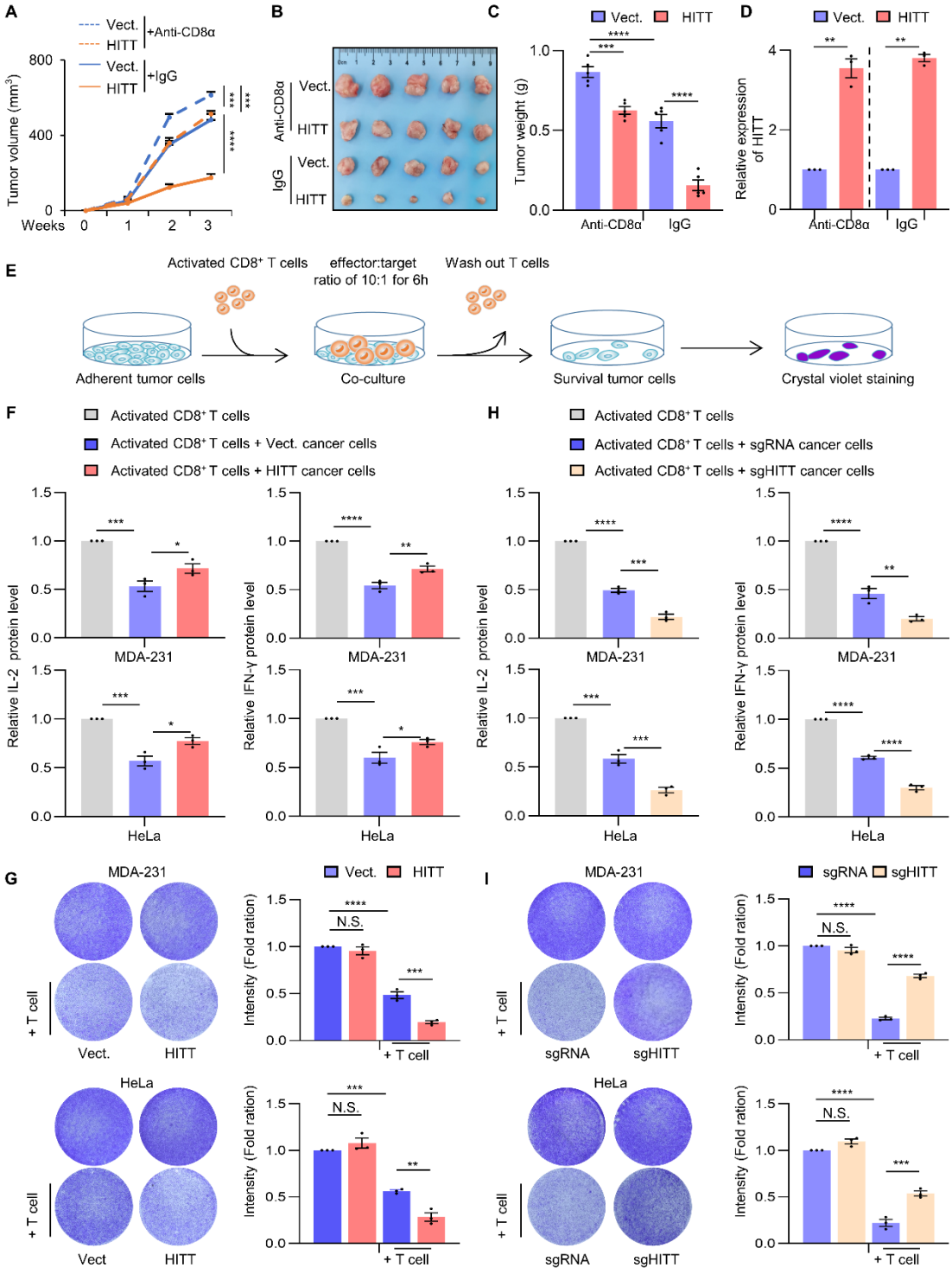

Figure 1 HITT sensitizes cancer cells to T cell-mediated cytotoxicity

(**A-C**) The volume (**A**), images (**B**) and the weight (**C**) of 4T1 syngeneic tumours. (**D**) The HITT levels in 4T1 syngeneic tumours determined by qRT-PCR. (**E**) Schematic of the crystal violet staining to analyze T-cell-mediated tumour cell-killing efficacy. (**F**) Detection of IL-2 and IFN-γ levels in the

supernatants of T cell and the control and HITT over-expressing MDA-231 and HeLa cell co-cultures by ELISA assays. (**G**) Detection of the attached MDA-231 and HeLa cell by crystal violet staining after co-culture with the activated T cells for 6h. The intensities were shown in bar graph (right). (**H**) Detection of IL-2 and IFN-γ levels in the supernatants of T cell and MDA-231 and HeLa cell co-cultures by ELISA assays. (**I**) Detection of the attached MDA-231 and HeLa cell by crystal violet staining after co-culture with the activated T cells for 6h. The intensities were shown in bar graph (right). Data in **A** and are shown as mean ± SD (n=5). Data in **C**, **D** and **F**-**I** are derived from three independent experiments shown as mean ± SEM. **P* < 0.05; ***P* < 0.01; ****P* < 0.001; ****P* < 0.0001; N.S. not significant by two-way ANOVA test (**A**) and one-way ANOVA test (**C** and **F**-**I**) and Student's t test (**D**).

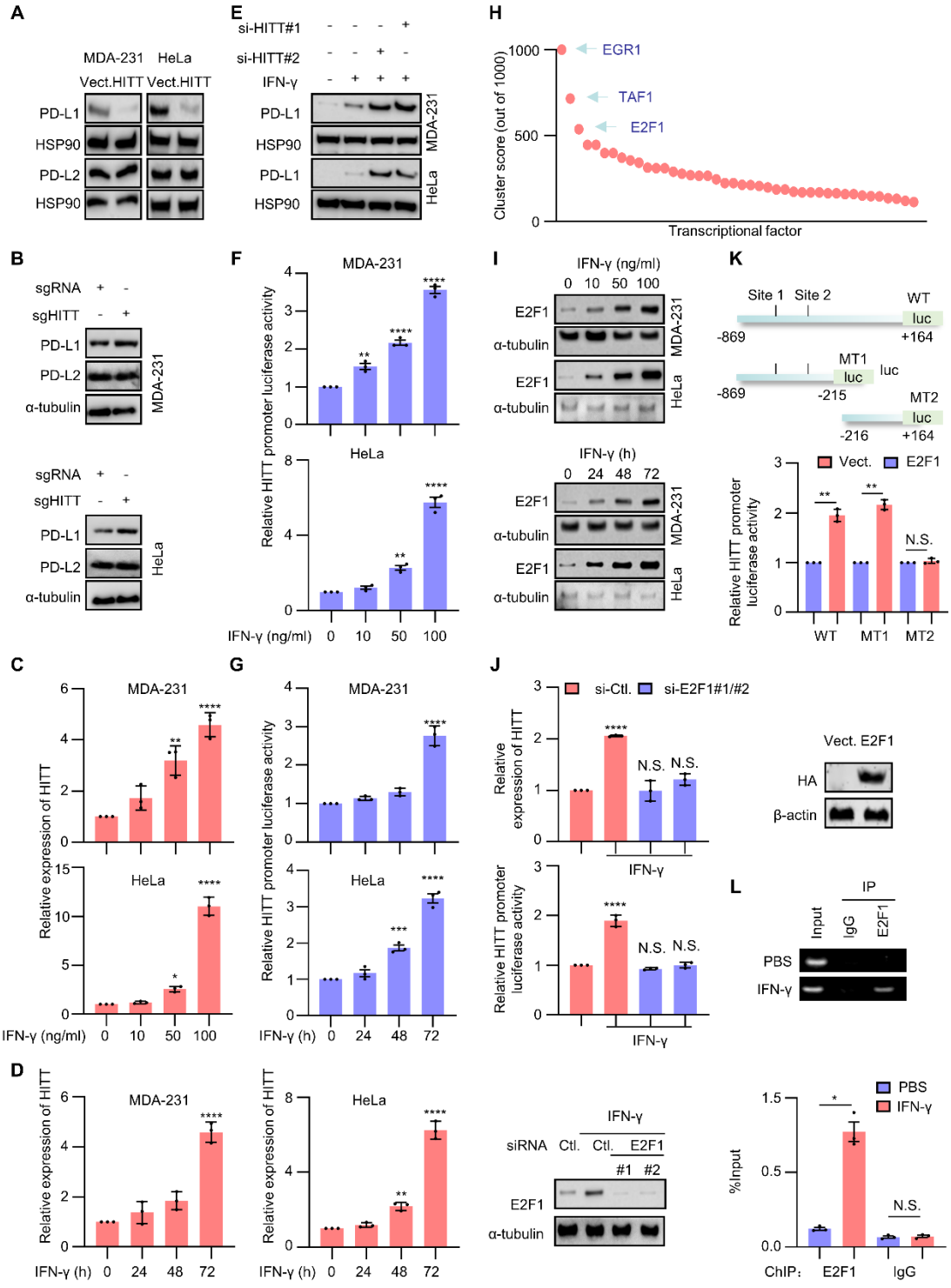

Figure 2 IFN-γ-induced and E2F1-mediated transactivation of HITT attenuates PD-L1 expression

(**A, B**) PD-L1 and PD-L2 protein levels analyzed by western blot (WB) assay in HITT stable overexpression (**A**) or HITT KO (**B**) cells. (**C**, **D**) HITT levels determined by qRT-PCR in MDA-231 and HeLa cells treated with different concentrations of IFN-γ for 24h (**C**) or treated with the indicated

time periods of 10ng/ml IFN-γ (**D**). (**E**) PD-L1 protein levels analyzed by WB in IFN-γ treated cells with or without HITT KD. (**F**, **G**) HITT promoter luciferase activities determined by luciferase reporter assay in MDA-231 and HeLa cells treated with different concentrations of IFN-γ for 24h (**F**) or the indicated time periods of 10ng/ml IFN-γ (**G**). (**H**) The relative binding potentials between different transcription factors and HITT promoter region were analyzed by UCSC ChIP sequence data. (**I**) E2F1 protein levels were detected by WB in MDA-231 and HeLa cells with different concentrations of IFN-γ for 24 h or with 10ng/ml IFN-γ for different time course. (**J**) HITT expression levels and HITT promoter luciferase activities were measured by qRT-PCR and luciferase reporter assay in IFN-γ (10ng/ml for 24h)-treated cells after E2F1 KD. E2F1 KD efficiency was validated by WB (bottom). (**K**) HITT promoter (Full-length, FL and MT) controlled luciferase activities were determined after transient transfection of the indicated reporter plasmids together with E2F1 expression plasmid. (**L**) The binding between HITT promoter region and E2F1 was determined by ChIP assay after IFN-γ treatment (10ng/ml for 24h). PCR band intensities were quantified using Image J and presented in the bar graph (bottom). Data are derived from three independent experiments shown as mean ± SEM. **P* < 0.05; ***P* < 0.01; ****P* < 0.001; *****P* < 0.0001; N.S. not significant by one-way ANOVA test (**C**, **D**, **F**, **G**, **J**) and Student's t test (**K**, **L**).

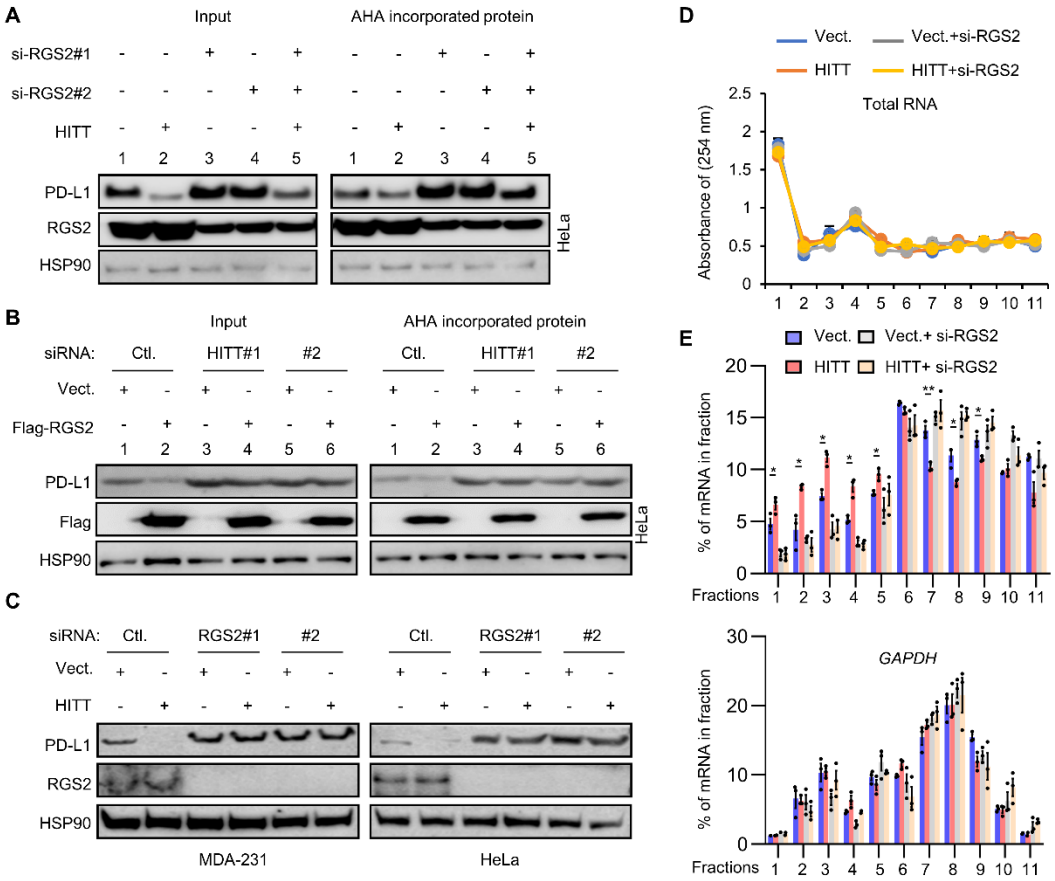

824

825 **Figure 3 HITT inhibits PD-L1 translation in a RGS2 dependent manner**

826 (**A**, **B**) Affinity purification of Biotinylated L-azidohomoalanine (AHA)-labeled acutely synthesized
827 proteins of PD-L1, RGS2 and HSP90 were detected by WB after HITT overexpression with or without
828 RGS2 KD (**A**) or RGS2 overexpression with or without HITT KD (**B**). (**C**) PD-L1 protein levels were
829 analyzed by WB in HITT stable lines with or without RGS2 KD. (**D**, **E**) Polysome in the cytoplasm
830 were fractionated through sucrose gradients. The total RNA amount was determined by the
831 intensity at 254 nm (**D**), and PD-L1 and GAPDH mRNA levels were detected by qRT-PCR (**E**) in
832 gradient fractions of HITT stable expression HeLa cells with or without RGS2 KD. Representative
833 data, as a percentage of total RNA of interest in the gradient from three independent experiments
834 are presented. **P* < 0.05; ***P* < 0.01 by Student's *t* test (**D**, **E**).

835

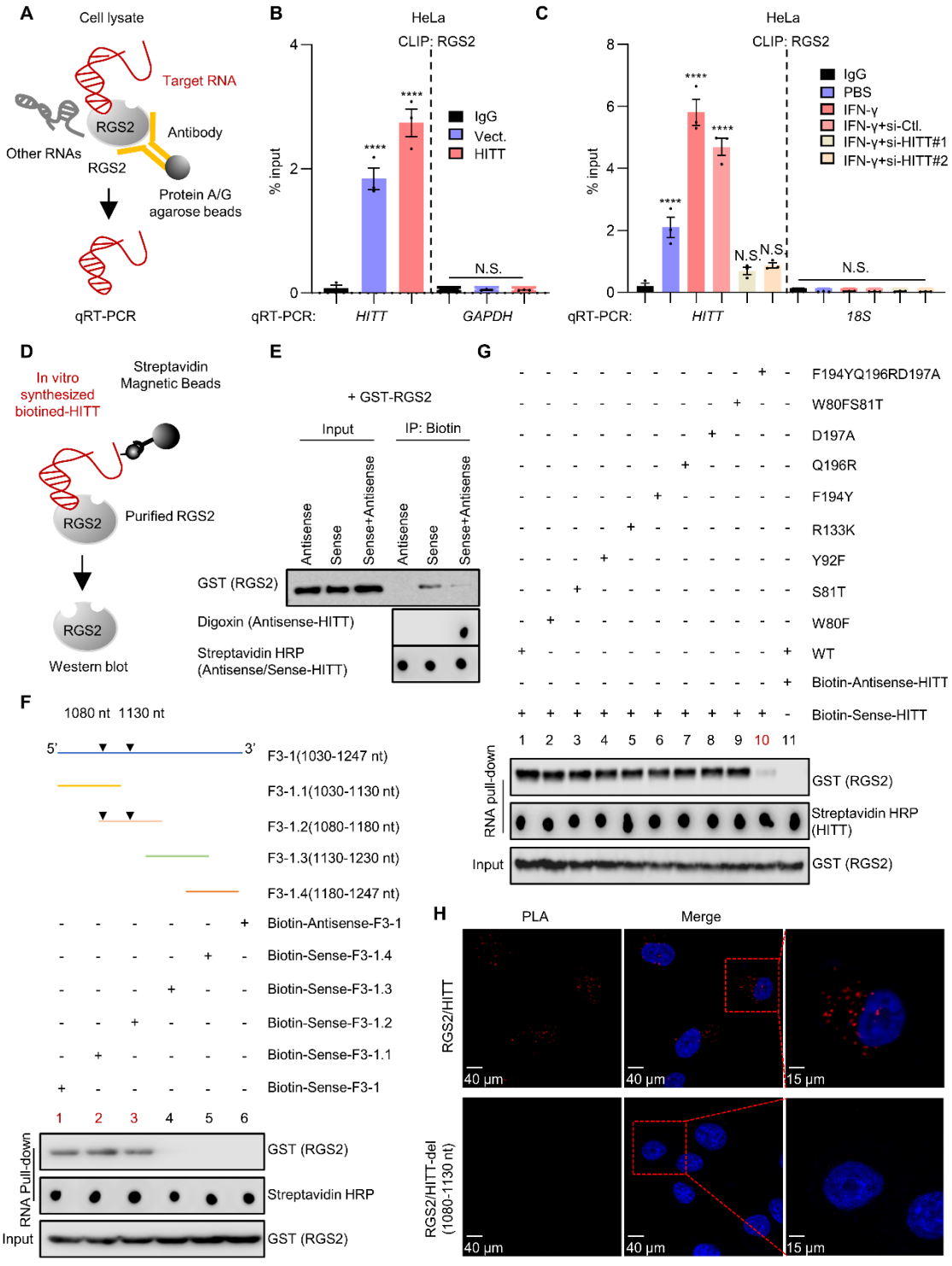

836

837 **Figure 4 RGS2 is a binding partner of HITT.**

838 (**A**) Schematic of CLIP assay for the binding between RGS2 and HITT in living cells. (**B, C**) HITT levels

839 determined by qRT-PCR following CLIP RGS2 after HITT overexpression (**B**), or KD in the presence

840 or absence of IFN-γ treatment (**C**) in HeLa cells, with GAPDH or 18s mRNA and CLIP IgG as negative

841 controls. (**D**) Schematic of in vitro RNA pull-down assay to analyze the binding between in vitro
842 synthesized Biotin-labeled HITT and purified RGS2. (**E**) GST-tagged RGS2 protein co-precipitated
843 with Biotin-Sense-HITT in the presence or absence of Digoxin-Antisense-HITT. (**F**) RGS2 protein co-
844 precipitated by Biotin-HITT-F3-1 (1030-1247 nt) or its fragments determined by RNA pull-down
845 assay. Schematic showing sequentially fragmented HITT-F3-1 (1030-1247 nt). (**G**) GST-tagged full
846 length RGS2 or its mutants co-precipitated with Biotin-Sense-HITT determined by WB. (**H**) PLA
847 analysis of endogenous RGS2/exogenous HITT or HITT-del (1080-1130 nt) in HeLa cells. Data
848 derived from three independent experiments are presented as mean ± SEM in the bar graph. ****P
849 < 0.0001; N.S. not significant by one-way ANOVA test (**B**, **C**). Scale bars: 40 μm and 15 μm.

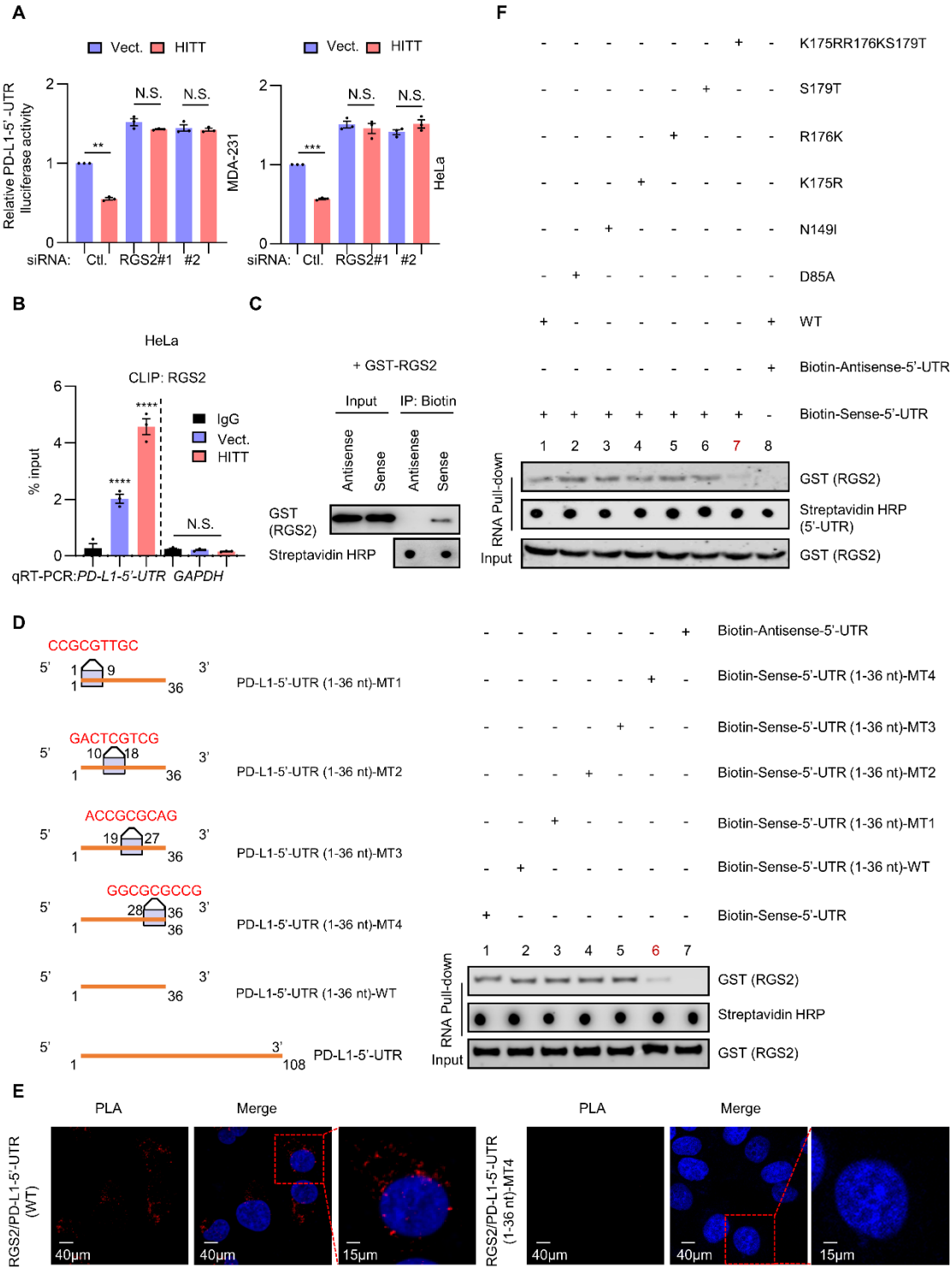

Figure 5 RGS2 physically binds with PD-L1-5'-UTR

(**A**) PD-L1-5'-UTR-driven luciferase activities determined in HITT stable lines with or without RGS2 KD. (**B**) PD-L1-5'-UTR levels determined by qRT-PCR following CLIP RGS2 in HITT overexpressing stable HeLa cells, with GAPDH mRNA and CLIP IgG as negative controls. (**C**) GST-tagged RGS2

protein co-precipitated with Biotin-PD-L1-5’-UTR or Biotin-PD-L1-5’-UTR antisense control determined by WB. (**D**) Schematic of the compensatory mutations in PD-L1-5’-UTR (1-36 nt). GST-tagged RGS2 protein co-precipitated with Biotin-PD-L1-5’-UTR (1-36 nt), or its mutants determined by RNA pull-down assay. (**E**) PLA analysis of endogenous RGS2/exogenous PD-L1-5’-UTR or 5’-UTR (1-36 nt) MT4 in HeLa cells. (**F**) GST-tagged RGS2 or mutant proteins co-precipitated with Biotin-PD-L1-5’-UTR (1-36 nt) determined by RNA pull-down assay. Data derived from three independent experiments are presented as mean ± SEM. $^{**}P < 0.01$; $^{***}P < 0.001$; $^{****}P < 0.0001$; N.S. not significant by Student’s t test (**A**) and one-way ANOVA test (**B**). Scale bars: 40 μm and 15 μm.

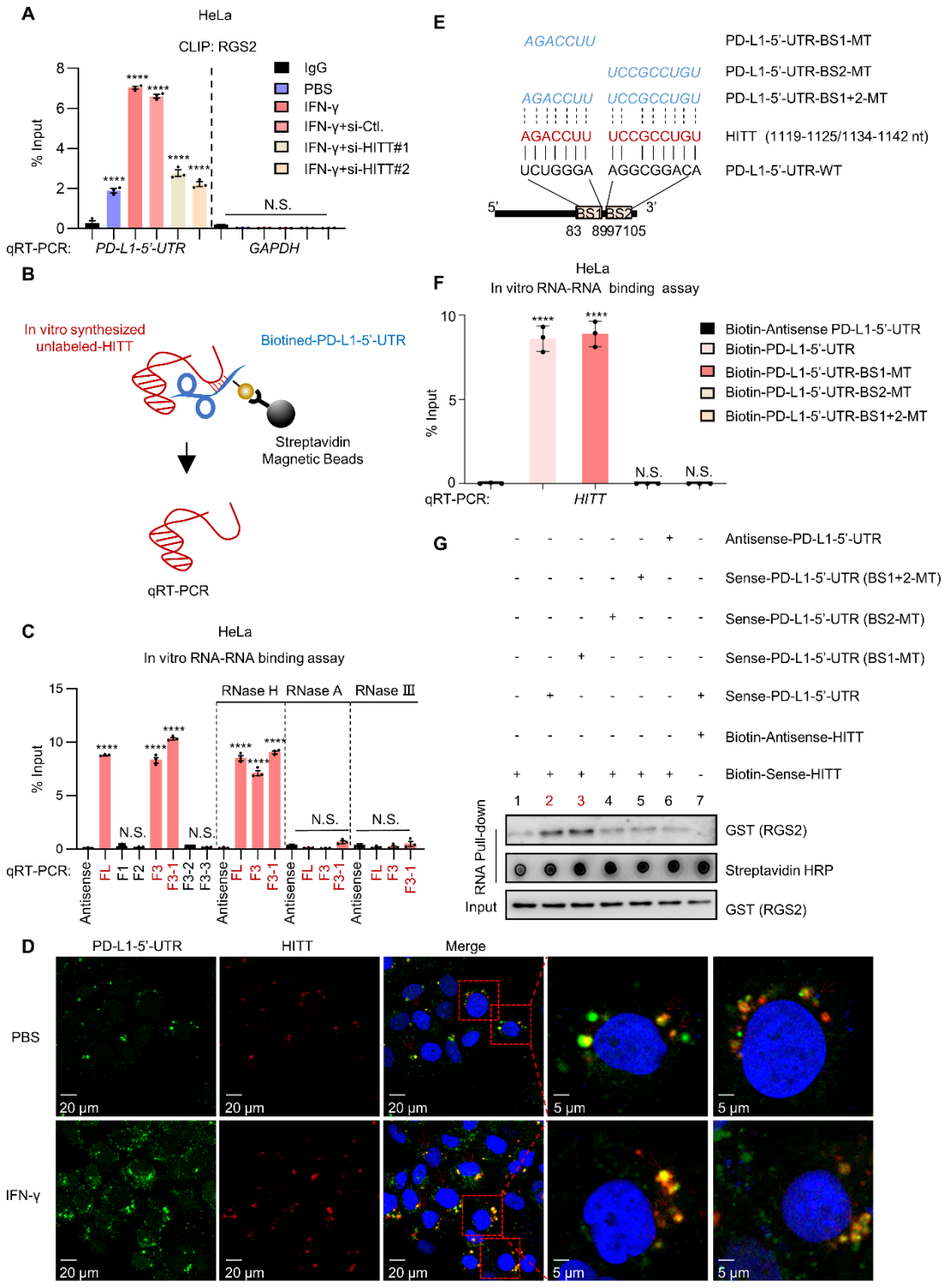

Figure 6 HITT forms RNA-RNA duplex with *PD-L1-5'*-UTR

(**A**) PD-L1-5'-UTR levels determined by qRT-PCR following CLIP RGS2 under IFN-γ treatment with or without HITT KD, with GAPDH mRNA and CLIP IgG as negative controls. (**B**) Schematic of in vitro RNA-RNA binding assay to detect the binding between in vitro synthesized unlabeled HITT and

Biotin-PD-L1-5’-UTR. (**C**) HITT and HITT fragments pulled down by Biotin-PD-L1-5’-UTR, Biotin-PD-L1-5’-UTR fragments or Biotin-antisense-PD-L1-5’-UTR control determined by qRT-PCR with or without RNase H, RNase A or RNase III. (**D**) FISH showing co-localization between HITT and PD-L1-5’-UTR in PBS or IFN-γ-treated HeLa cells. (**E**) Schematic of the complementary sequence (binding sites, BS) between HITT and PD-L1-5’-UTR according to the prediction of an online bioinformatic tool (rna.informatik.uni-freiburg.de/IntaRNA/Input.jsp). Three PD-L1-5’-UTR mutations, which lost the complementarity site of PD-L1-5’-UTR at BS1 (BS1-MT), BS2 (BS2-MT) and both BS1 and BS2 (BS1+2-MT) were generated and shown in diagram. (**F**) HITT co-precipitated by Biotin-PD-L1-5’-UTR (WT or mutants) or Biotin-Antisense-PD-L1-5’-UTR control determined by qRT-PCR. (**G**) GST-tagged RGS2 pulled down by Biotin-HITT and Biotin-Antisense-HITT control in the presence of unlabeled FL PD-L1-5’-UTR or PD-L1-5’-UTR mutants determined by WB in an in vitro RNA pull-down assay. Data derived from three independent experiments are presented as mean ± SEM. ****$P < 0.0001$; N.S. not significant by one-way ANOVA test (**A**, **C**, **F**). Scale bars: 20 μm and 5 μm.

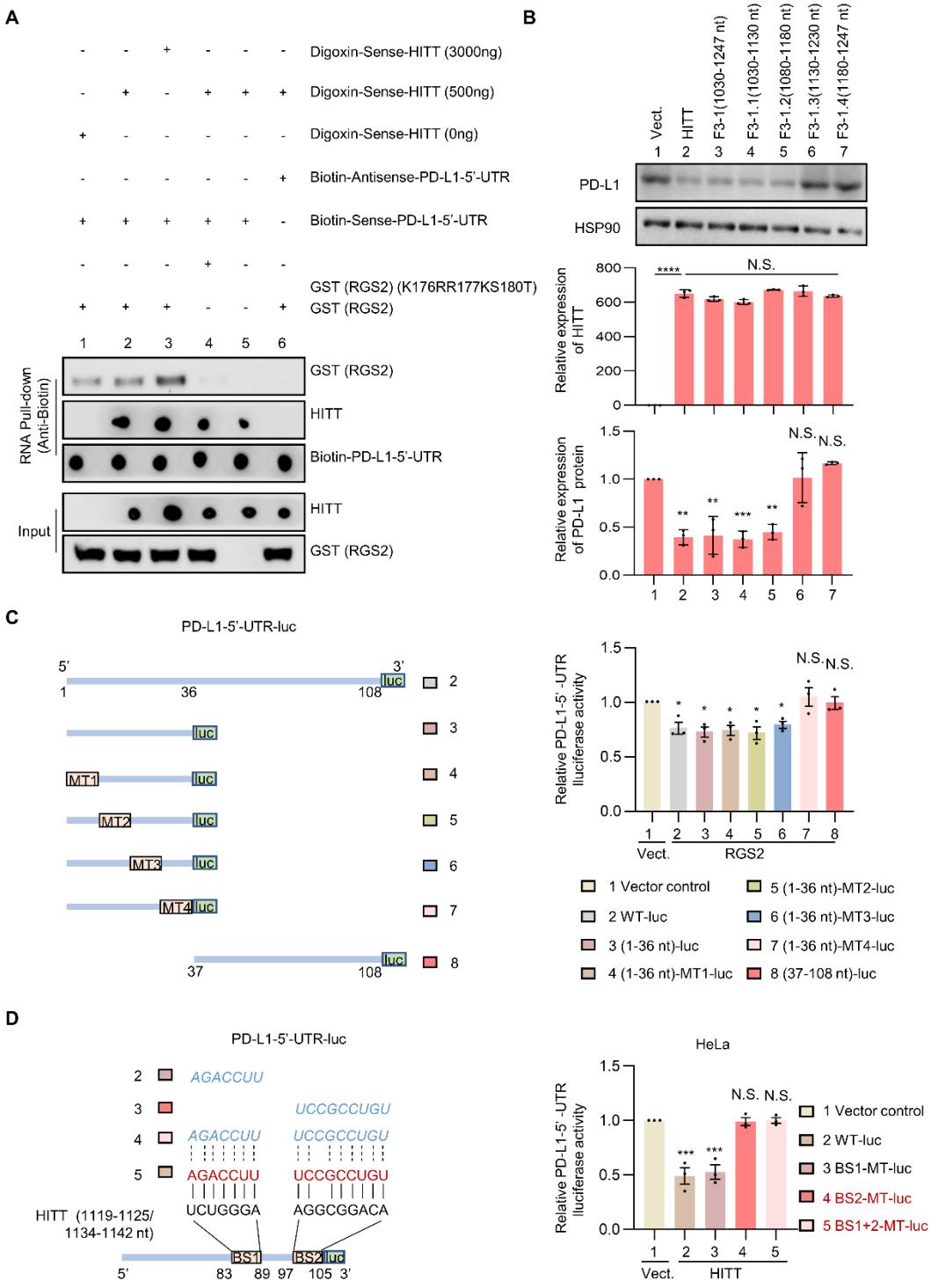

883

884 **Figure 7 RGS2/HITT/PD-L1-5'-UTR interaction is required for PD-L1 inhibition**

885 (**A**) The interactions between RGS2/HITT/PD-L1-5'-UTR RNA determined by RNA pull-down assays.

886 (**B**) PD-L1 protein levels after transfection HITT, F3-1, F3-1.1, F3-1.2, F3-1.3 and F3-1.4 into HeLa

887 cells. HITT and its mutant overexpression efficiencies were measured by qRT-PCR (middle) and the

888 PD-L1 intensities were quantified and shown in bar graph (bottom). (**C** and **D**) The reporter
889 activities of the indicated luciferase reporters before and after RGS2 overexpression (**C**) or HITT
890 overexpression (**D**). Data derived from three independent experiments are presented as mean ±
891 SEM.*P < 0.05; **P < 0.01; ***P < 0.001; ****P < 0.0001; N.S. not significant by one-way ANOVA
892 test (**B**-**D**).
893

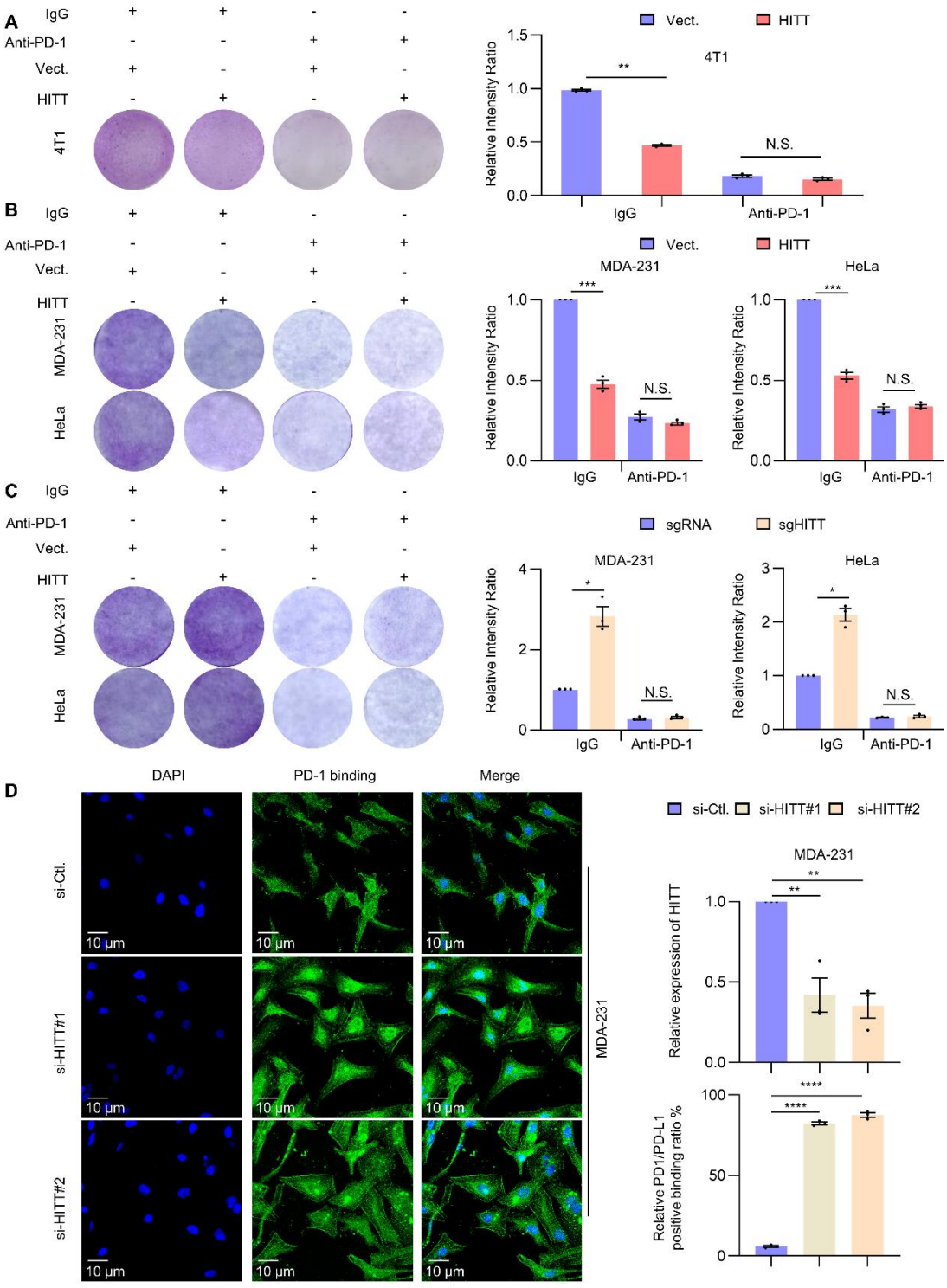

Figure 8 HITT enhances T-cell-mediated tumour cell-killing efficacy in a PD-L1-dependent manner

(**A**) Detection of the attached 4T1-OVA cells by crystal violet staining after co-culture with the activated mouse OT-I T cells for 2 days in the presence of anti-PD-1 antibody or IgG control. The intensities were shown in bar graph. (**B, C**) Detection of the attached MDA-231 and HeLa cells by

crystal violet staining after co-culture with the activated T cells for 6h in the presence of anti-PD-1 antibody or IgG control. The intensities were shown in bar graph (right). (**D**) Immunostaining of PD-1 (fused to Ig-Fc) on HITT KD MDA-231 cells. PD-L1 fluorescences intensity at cell edge were quantified and the relative levels were shown in bar graph (right). HITT KD efficiency was determined by qRT-PCR (right). Data derived from three independent experiments are presented as mean ± SEM. *P < 0.05; **P < 0.01; *** P < 0.001; **** P < 0.0001; N.S. not significant by Student's t test (**A**-**C**) and one-way ANOVA test (**D**). Scale bars: 10 μm.

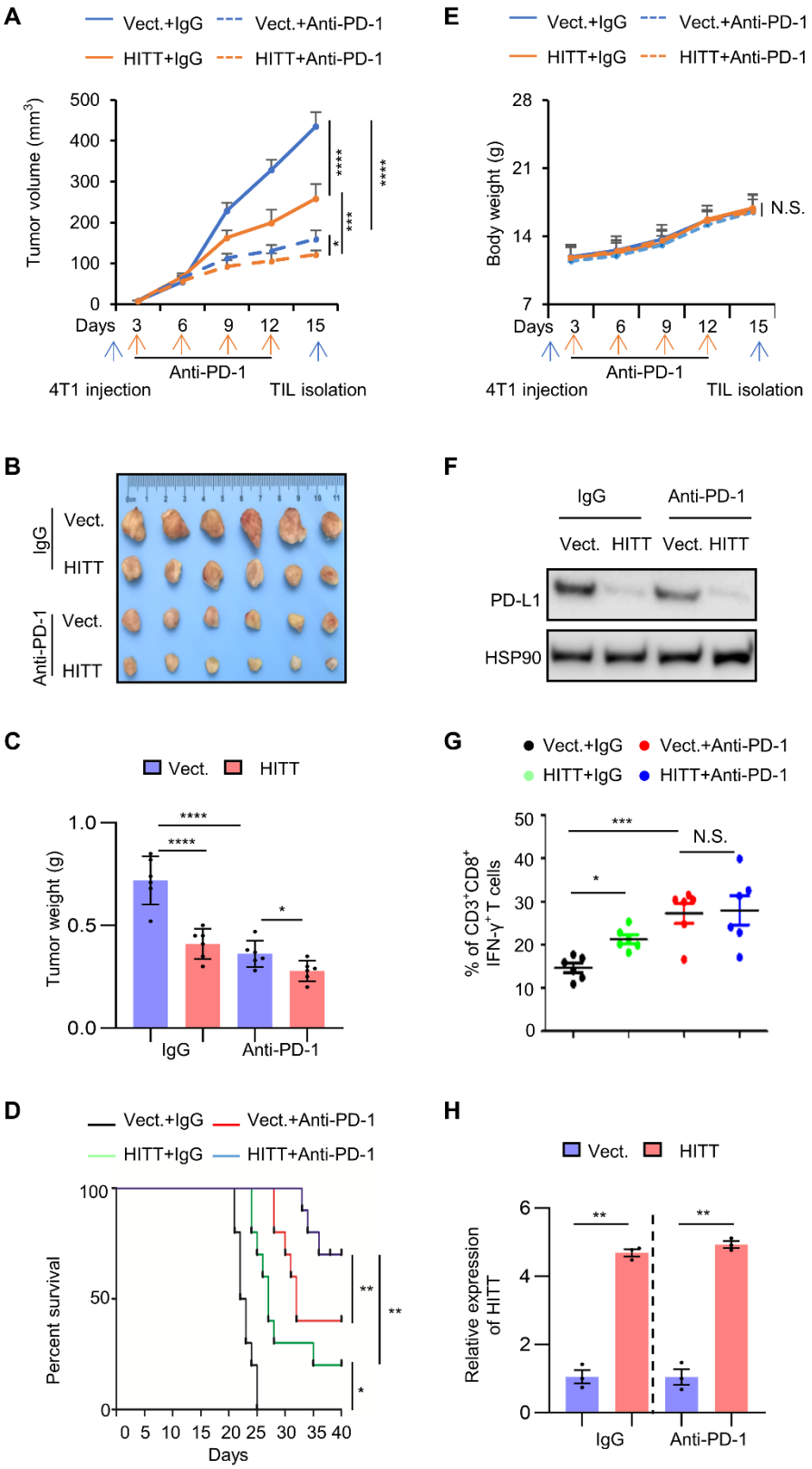

Figure 9 HITT inhibits tumour growth by attenuating PD-L1-medaited T cell deactivation in vivo.

(**A-C**) The volume(**A**), images (**B**) and the tumor weight (**C**). Each dot represents an evaluation in an individual tumor. (**D**) The Kaplan-Meier survival curve of mice bearing syngeneic 4T1 tumour with the treatment of IgG or anti-PD-1. (**E**) The body weights of BALB/c mice measured along the treatments. (**F**) The PD-L1 protein levels determined by WB. (**G**) Immunostaining of $CD8^+$ IFN-γ^+ in the $CD3^+$ T cell populations from the isolated tumour-infiltrating lymphocytes in syngeneic tissues. Each dot represents an evaluation in an individual tumor. (**H**) The HITT levels in 4T1 syngeneic determined by qRT-PCR. Data in **A**, **C**-**E** and **G** are shown as mean ± SD. **P* < 0.05; ***P* < 0.01; ****P* < 0.001; ****P* < 0.0001; N.S. not significant by two-way ANOVA test (**A**, **E**, n=6 mice per group) and one-way ANOVA test (**C**, **G**, n=6 mice per group) and the log-rank test (**D**, n = 10 mice per group) and Student's t test (**H**). Data derived from three independent experiments are presented as mean ± SEM.

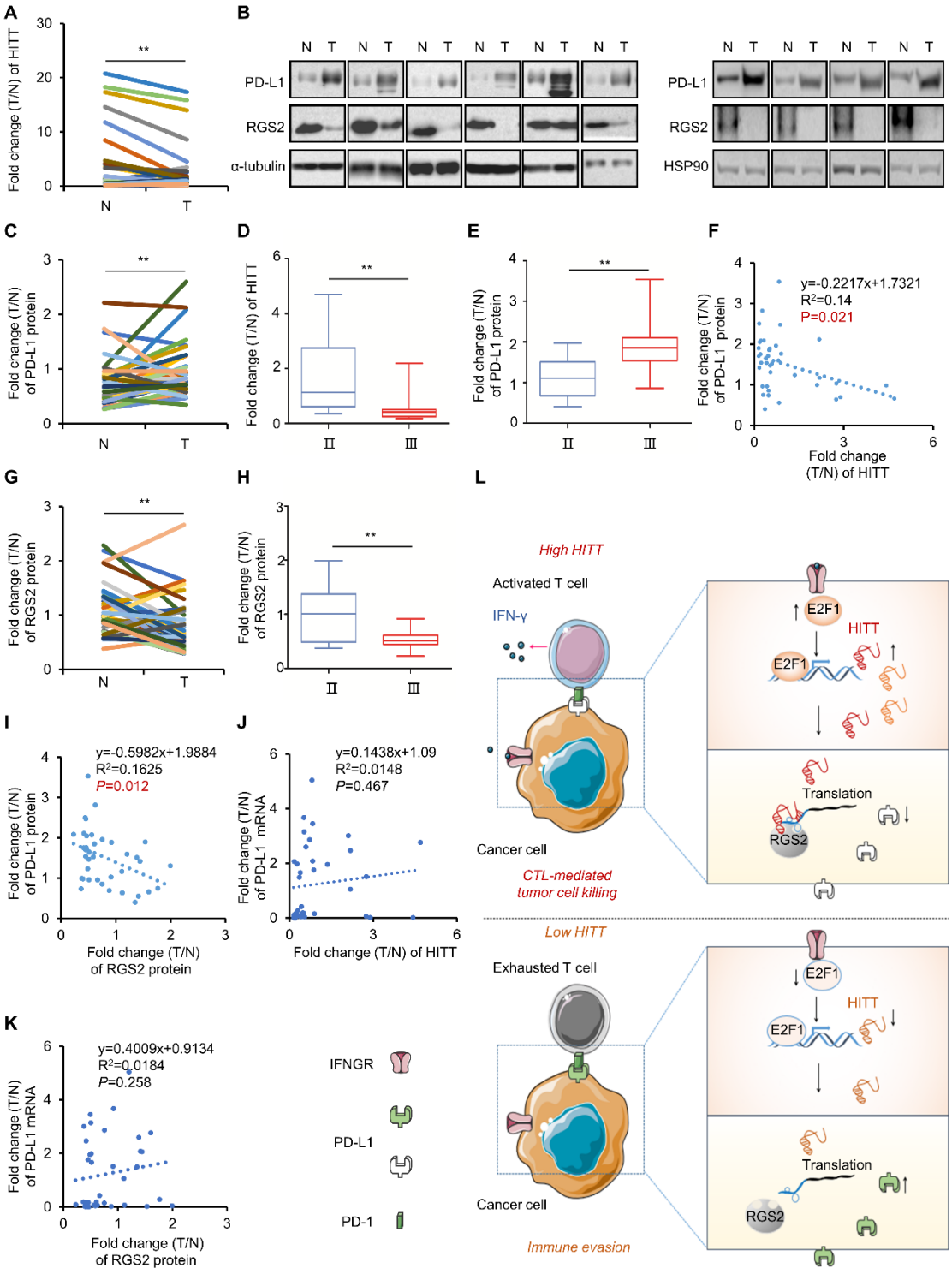

Figure 10 RGS2/HITT/PD-L1 are associated with each other in vivo

(**A**) The expression of HITT in human breast tumours (T) and their paired adjacent normal controls (N) (n = 38) determined by qRT-PCR. (**B, C**) Representative WB (**B**) and quantification of PD-L1 proteins (**C**) in 38 of breast cancers and their adjacent normal controls. (**D, E**) The correlation

between the fold-change of HITT (**D**)/PD-L1 protein (**E**) and TNM stages. (**F**) The lineal correlation analysis of the fold-change of HITT expression vs those of PD-L1 protein expression (*P*=0.021). (**G**) Quantification of RGS2 proteins in 38 of breast cancers and their adjacent normal controls. (**H**) The correlation between the fold-change of RGS2 protein and TNM stages. (**I**) The lineal correlation analysis of the fold-change of RGS2 protein expression vs those of PD-L1 protein expression (*P*=0.012). (**J**) The lineal correlation analysis of the fold-change of HITT expression vs those of PD-L1 mRNA expression. (**K**) The lineal correlation analysis of the fold-change of RGS2 protein expression vs those of PD-L1 mRNA expression. (**L**) Schematic diagram of RGS2/HITT/PD-L1 regulated interaction between cancer cells and T cells to modulate tumour immunity. IFN-γ secreted by activated T cell or others triggers E2F1-mediated transactivation of lncRNA HITT in cancer cells, where HITT directly binds with RGS2 and PD-L1-5'-UTR. This function of HITT also strengths the direct interaction between RGS2 and PD-L1-5'-UTR. These interactions among HITT, RGS2 and PD-L1-5'-UTR leads to a retarded translation of PD-L1, and elevated T cell activation. Such activity of HITT is impaired in cancer cells due to the reduced expression of HITT, Activating HITT in cancer cells is a potential treatment to elevate T cell immunity. Data derived from three independent experiments are presented as mean ± SEM (**A**, **C**-**K**). $^{**}P < 0.01$ by Student's t test (**A**, **C**-**E**, **G** and **H**). Correlations were calculated according to Pearson correlation (**F**, **I**-**K**).